

Switching Gradient Directions for Query-Efficient Black-Box Adversarial Attacks

Chen Ma¹, Shuyu Cheng², Li Chen¹, Junhai Yong¹

¹School of Software, BNRist, Tsinghua University, Beijing 100084, China

²Dept. of Comp. Sci. and Tech., BNRist Center, Institute for AI, THBI Lab, Tsinghua University, Beijing 100084, China
{mac16,chengsy18}@mails.tsinghua.edu.cn, {chenlee,yongjh}@tsinghua.edu.cn

Abstract

We propose a simple and highly query-efficient black-box adversarial attack named SWITCH, which has a state-of-the-art performance under ℓ_2 and ℓ_∞ norms in the score-based setting. In the black box attack setting, designing query-efficient attacks remains an open problem. The high query efficiency of the proposed approach stems from the combination of transfer-based attacks and random-search-based ones. The surrogate model’s gradient \hat{g} is exploited for the guidance, which is then switched if our algorithm detects that it does not point to the adversarial region by using a query, thereby keeping the objective loss function of the target model rising as much as possible. Two switch operations are available, *i.e.*, SWITCH_{neg} and SWITCH_{rnd}. SWITCH_{neg} takes $-\hat{g}$ as the new direction, which is reasonable under an approximate local linearity assumption. SWITCH_{rnd} computes the gradient from another model, which is randomly selected from a large model set, to help bypass the potential obstacle in optimization. Experimental results show that these strategies boost the optimization process whereas following the original surrogate gradients does not work. In SWITCH, no query is used to estimate the gradient, and all the queries aim to determine whether to switch directions, resulting in unprecedented query efficiency. We demonstrate that our approach outperforms 10 state-of-the-art attacks on CIFAR-10, CIFAR-100 and TinyImageNet datasets. SWITCH can serve as a strong baseline for future black-box attacks. The PyTorch source code is released in <https://github.com/machanic/SWITCH>.

Introduction

Adversarial attacks are the major security threat to deep neural networks (DNNs) that add human-imperceptible perturbations to benign images for the misclassification of DNNs. Adversarial attacks can be divided into two main categories based on whether the internal information of the target model is exposed to the attacker, *i.e.*, white-box and black-box attacks. Black-box attacks are more realistic in real-world systems because they do not require the parameters and gradients of the target model. Many methods have been proposed to craft adversarial examples under the black-box attack setting. These methods can be divided into transfer- and query-based attacks.

Transfer-based attacks generate adversarial examples by attacking a pre-trained surrogate model to fool the target model (Liu et al. 2017; Papernot, McDaniel, and Goodfellow 2016; Demontis et al. 2019; Huang et al. 2019).

Transfer-based attacks have practical value because they do not require querying the target model. However, the attack success rate is low in the following situations: (1) targeted attack, and (2) the network structures of the surrogate model and target model have a large difference. The success rate is low in these situations because of the incorrect gradient provided by the surrogate model. This gradient could frequently point to a non-adversarial region of target model, following this direction consecutively in the optimization leads to a fail attack. Hence, it should be considered to switch the gradient direction when it deviates from the correct direction.

Query-based attacks require an oracle access to the target model, and we focus on the score-based attack setting which requires accessing to the loss function value. Some score-based attacks (Chen et al. 2017; Tu et al. 2019; Ilyas et al. 2018a; Ilyas, Engstrom, and Madry 2019) estimate an approximate gradient by querying the target model at multiple points. However, the high query complexity is inevitable in estimating the approximate gradient with high precision. To reduce the query complexity, another type of query-based attacks, *i.e.*, random-search-based attacks (Guo et al. 2019; Andriushchenko et al. 2020), eliminates the gradient estimation and turns to sampling a random perturbation at each iteration, which is either added to or subtracted from the target image. Then, the modified image is fed to the target model to compute a loss value. If the loss value peaks a historical high, the attacker accepts the perturbation; otherwise, it is rejected. The main issue of this strategy is that the sampled perturbation does not incorporate the gradient information, thereby leading to a high rejection rate and inefficient optimization. In addition, nothing is done if the perturbation is rejected, resulting in many wasted queries. Thus, it is worth exploring how to incorporate the gradient information to enhance the optimization’s efficiency.

In this study, we propose a novel black-box adversarial attack named SWITCH that bridges the gap between transfer-based attacks and random-search-based ones to improve the query efficiency. SWITCH incorporates the gradient of a surrogate model because of its informative guidance. However, the surrogate gradient is not the same as that of the target model’s gradient and thus does not always point to the adversarial region of the target model. To reduce the incorrect updates, SWITCH makes a temporary image by perturbing the target image towards the surrogate gradient. This

temporary image and its label are fed to the target model to compute a loss value. If the loss is not increased from the last iteration, SWITCH switches to a new direction. This new direction is obtained by either taking a negative sign for the surrogate gradient (SWITCH_{neg} algorithm), or computing a new gradient of another surrogate model, which is randomly selected from a large model set (SWITCH_{rnd} algorithm). Finally, the target image is updated by using the switched gradient. Thus, in each iteration, the algorithm aims to keep the loss function increasing by switching the gradient. Both the attack success rate and query efficiency are improved because the switched direction could avoid following the wrong direction and consequently bypass the potential obstacle in optimization. Furthermore, SWITCH_{rnd} uses the random selection in a large model set for computing the new gradient, which is beneficial for the exploration because it ensembles the guidances of multiple models to avoid following a potentially inferior model.

We evaluate the proposed method on the CIFAR-10 (Krizhevsky, Hinton et al. 2009), CIFAR-100 (Krizhevsky, Hinton et al. 2009) and TinyImageNet (Russakovsky et al. 2015) datasets and compare it with 10 state-of-the-art query-based black-box attacks. The results show that the proposed approach requires the fewest queries to perform a successful attack, which significantly outperforms other methods. For example, the proposed approach makes no more than nine queries in the untargeted attacks under ℓ_2 norm constraint, whereas others require hundreds. Therefore, SWITCH achieves new state-of-the-art performance.

The main contributions of this study are as follows.

(1) We propose a simple and highly query-efficient black-box attack named SWITCH to bridge the gap between transfer-based attacks and random-search-based ones to overcome their shortcomings. The proposed approach switches the gradient to avoid following the wrong direction and consequently bypass the potential obstacle in optimization, which keeps the loss function increasing as much as possible.

(2) Despite its simplicity, SWITCH spends extremely fewer queries than state-of-the-art methods on the CIFAR-10, CIFAR-100 and TinyImageNet datasets. We consider the proposed method to be a strong baseline for future attacks.

Background

Black-box attacks. It is unrealistic to obtain internal information of target models in many real-world systems, thus many studies focus on performing attacks in the black-box setting. Black-box attacks can be divided into transfer- and query-based attacks. In transfer-based attacks (Liu et al. 2017; Papernot, McDaniel, and Goodfellow 2016; Demontis et al. 2019; Huang et al. 2019), adversarial examples generated by attacking a surrogate model might remain adversarial for the target model. Given that targeted attack is difficult for transfer-based attacks, certain methods use the ensemble of surrogate models (Liu et al. 2017) or exploit intermediate feature maps (Inkawhich et al. 2019) to improve the success rate. However, the attack success rate remains unsatisfactory and new types of attacks can be detected easily by using meta-learning-based detector (Ma et al. 2019).

Query-based attacks can be further divided into decision- and score-based attacks based on the type of information returned from the target model to the attacker. In decision-based attacks (Dong et al. 2019; Cheng et al. 2020), the attacker only knows the output label of the target model. In this study, we focus on the score-based attack, in which the attacker can obtain the output scores of the target model. Although the true gradient cannot be directly obtained in black-box attacks, we can still optimize the adversarial examples by using the approximate gradients. Early studies (Chen et al. 2017; Bhagoji et al. 2018) estimate the approximate gradient by sampling from a noise distribution around the pixels, which is expensive because each pixel needs two queries. To reduce the query complexity, methods are improved by incorporating data and time prior information (Ilyas, Engstrom, and Madry 2019), using meta-learning to learn a simulator (Ma, Chen, and Yong 2020), searching the solution among the vertices of the ℓ_∞ ball (Moon, An, and Song 2019), and searching the adversarial perturbation on a low-dimensional embedding space (Huang and Zhang 2020; Tu et al. 2019). Different from the methods that estimate gradients, random-search-based attacks (Guo et al. 2019; Andriushchenko et al. 2020) sample a random perturbation with the values filled with the maximum allowed perturbation ϵ or $-\epsilon$, which is either added to or subtracted from the target image. Then, the modified image is fed to the target model to determine whether to accept the perturbation. This type of methods significantly reduces the query complexity because they directly find the solution among the extreme points in ℓ_p ball and do not require the high-cost gradient estimation. However, the sampled perturbation does not encode the gradient information, resulting in inefficient optimization. In contrast, the proposed method exploits the gradient of the surrogate model and then switches the direction when necessary to keep the loss increasing as much as possible, thereby achieving high attack success rate and query efficiency.

Adversarial Setup. Given the target model f and input-label pair (\mathbf{x}, y) , which is correctly classified by f . The adversarial example \mathbf{x}_{adv} is produced by $\mathbf{x}_{\text{adv}} = \mathbf{x} + \delta$ that satisfies $\|\mathbf{x}_{\text{adv}} - \mathbf{x}\|_p \leq \epsilon$, where ϵ is a predefined maximum allowed distance, and δ is the small perturbation. The goal is to find \mathbf{x}_{adv} that maximizes the attack objective loss function $\mathcal{L}(\cdot, \cdot)$, which can be the cross-entropy loss or the max-margin logit loss. The projected gradient descent (PGD) attack (Madry et al. 2018) iteratively updates adversarial examples as $\mathbf{x}_{t+1} = \prod_{\mathcal{B}_p(\mathbf{x}, \epsilon)}(\mathbf{x}_t + \eta \cdot \mathbf{g})$, where \prod is the projection operation, $\mathcal{B}_p(\mathbf{x}, \epsilon)$ is the ℓ_p ball centered at \mathbf{x} with radius ϵ , η is the learning rate, and \mathbf{g} is the normalized gradient under ℓ_p norm, *i.e.*, $\mathbf{g} = \frac{\nabla_{\mathbf{x}_t} \mathcal{L}(f(\mathbf{x}_t), y)}{\|\nabla_{\mathbf{x}_t} \mathcal{L}(f(\mathbf{x}_t), y)\|_2}$ under ℓ_2 norm and $\mathbf{g} = \text{sign}(\nabla_{\mathbf{x}_t} \mathcal{L}(f(\mathbf{x}_t), y))$ under ℓ_∞ norm. In this study, we also follow above steps to update the adversarial image, except that \mathbf{g} is replaced with the surrogate gradient or the switched one.

Method

The proposed algorithm is shown in Algorithm 1 and Fig. 1. In each iteration, the algorithm first feeds current image \mathbf{x}_{adv} and its label t to a pre-trained surrogate model m , where

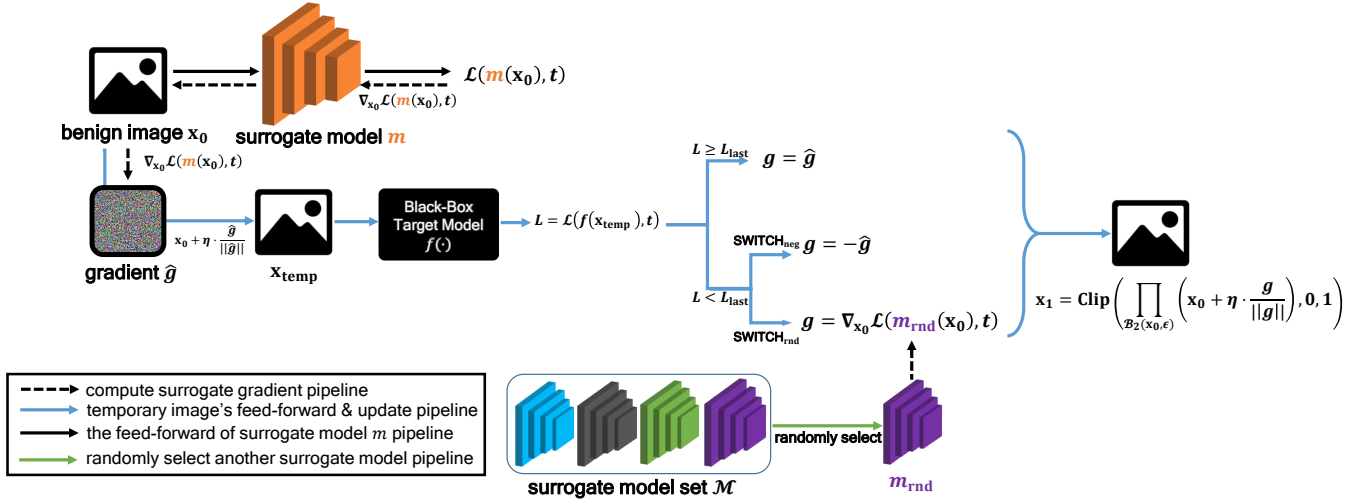


Figure 1: The first attack iteration of SWITCH under ℓ_2 norm constraint (detailed in Algorithm 1), where L_{last} (initialized as $L_{\text{last}} = \mathcal{L}(f(x_0), t)$) indicates the loss value of the last iteration. In each iteration, the algorithm makes temporary image x_{temp} by taking the gradient ascent step with surrogate gradient \hat{g} . Then, loss value L is computed by feeding x_{temp} to the target model. If $L < L_{\text{last}}$, the algorithm must switch the gradient direction; otherwise, it accepts \hat{g} . Two switch operation options are available, namely, SWITCH_{neg} and SWITCH_{rnd}, which either take the reverse direction or compute a new gradient on another surrogate model. Finally, the adversarial example x_1 for the next iteration is produced using the switched direction g .

x_{adv} is initialized as the benign image and updated iteratively. To optimize x_{adv} , the attack objective loss, which is adopted as max-margin logit loss (Carlini and Wagner 2017) (Eqn. 1), is maximized during attack.

$$\mathcal{L}(\hat{y}, t) = \begin{cases} \max_{j \neq t} \hat{y}_j - \hat{y}_t, & \text{if untargeted attack;} \\ \hat{y}_t - \max_{j \neq t} \hat{y}_j, & \text{if targeted attack;} \end{cases} \quad (1)$$

\hat{y} is the logits output of the model, t is the target class y_{adv} in the targeted attack and the true class y in the untargeted attack, and j indexes the other classes. Then, the gradient of the surrogate model m 's loss w.r.t. x_{adv} is computed as $\hat{g} \leftarrow \nabla_{x_{\text{adv}}} \mathcal{L}(m(x_{\text{adv}}), t)$. Sometimes, directly following \hat{g} could not increase the loss because \hat{g} deviates too much from the true gradient. SWITCH proposes to query the loss value to detect such situations and switch to a new direction. We propose two variants, namely SWITCH_{neg} and SWITCH_{rnd}, which use different strategies to determine the new direction.

SWITCH_{neg} is motivated by the approximate linearity assumption of DNNs (Goodfellow, Shlens, and Szegedy 2015). Assuming the target model f is locally linear at the current point x_{adv} , then the loss value increases along the $-\hat{g}$ direction if it decreases along the \hat{g} direction for any direction \hat{g} . Fig. 2 illustrates the case: the loss will decrease along \hat{g} direction if $\hat{g} \cdot \nabla_{x_{\text{adv}}} \mathcal{L}(f(x_{\text{adv}}), t) < 0$. However, the inner product of $-\hat{g}$ and $\nabla_{x_{\text{adv}}} \mathcal{L}(f(x_{\text{adv}}), t)$ is positive, and then $-\hat{g}$ is the rising direction of loss function. Therefore, SWITCH_{neg} feeds $x_{\text{adv}} + \eta \cdot \frac{\hat{g}}{\|\hat{g}\|_2}$ to f to compute a loss value L . If L is increased from the last iteration, we accept \hat{g} ; otherwise, we switch to the negative gradient $-\hat{g}$. Once the final gradient is selected, we update the image x_{adv} and then project it to ℓ_p -ball with a radius of ϵ . Finally, we record

¹In ℓ_∞ norm attack, it should change to $x_{\text{adv}} + \eta \cdot \text{sign}(\hat{g})$

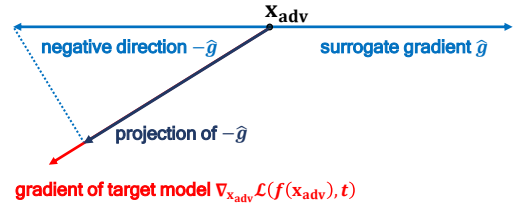


Figure 2: Illustration of SWITCH_{neg}, where x_{adv} is the current image to be updated. When the target model f is locally approximately linear, the loss should increase along $-\hat{g}$ direction if it decreases along \hat{g} direction.

the loss value L_{last} of the updated x_{adv} , which is used for the next iteration to distinguish whether the loss increases or decreases.

In certain difficult scenarios, the approximate linearity assumption does not necessarily hold even locally. In this situation, both directions of \hat{g} and $-\hat{g}$ cannot increase the loss value. In practice, when such situation happens, the current surrogate model m is less useful, however other models would help, which leads to SWITCH_{rnd}. A possible explanation is that in some hard cases, consecutively following the gradient of one surrogate model could make it more and more useless during the optimization. For example, the surrogate gradient maintains a similar direction, but there seems to be an obstacle in this direction. However, other directions could still be useful, so selecting a gradient from another surrogate model could bypass the obstacle in optimization. We build a large set of surrogate models for the selection, because random selection in a large set of surrogate models is beneficial for the exploration, and the effectiveness of this strategy is validated in Subspace Attack (Yan, Guo,

Algorithm 1 SWITCH Attack under ℓ_2 norm constraint

Input: Input image \mathbf{x} , true class label y of \mathbf{x} , target class label y_{adv} , feed-forward function f of the target model, a surrogate model m , a set of surrogate models \mathcal{M} , attack objective loss function $\mathcal{L}(\cdot, \cdot)$ defined in Eqn. 1.

Parameters: image learning rate η , the radius ϵ of ℓ_2 -norm ball, switch strategy $t \in \{\text{negative, random}\}$.

Output: \mathbf{x}_{adv} that satisfies $\|\mathbf{x}_{adv} - \mathbf{x}\|_2 \leq \epsilon$.

```

1: if targeted attack then
2:    $t \leftarrow y_{adv}$ 
3: else
4:    $t \leftarrow y$ 
5: end if
6:  $L_{last} \leftarrow \mathcal{L}(f(\mathbf{x}), t)$ 
7: Initialize the adversarial example  $\mathbf{x}_{adv} \leftarrow \mathbf{x}$ 
8: while not successful do
9:    $\hat{\mathbf{g}} \leftarrow \nabla_{\mathbf{x}_{adv}} \mathcal{L}(m(\mathbf{x}_{adv}), t)$ 
10:   $\mathbf{x}_{temp} \leftarrow \mathbf{x}_{adv} + \eta \cdot \frac{\hat{\mathbf{g}}}{\|\hat{\mathbf{g}}\|_2}$   $\triangleright$  replacing this line with
 $\mathbf{x}_{temp} \leftarrow \mathbf{x}_{adv} + \eta \cdot \text{sign}(\hat{\mathbf{g}})$  for  $\ell_\infty$  norm attack.
11:   $L \leftarrow \mathcal{L}(f(\mathbf{x}_{temp}), t)$ 
12:  if  $L \geq L_{last}$  then
13:     $\mathbf{g} \leftarrow \hat{\mathbf{g}}$   $\triangleright$  accept this gradient directly
14:  else
15:    if  $t = \text{negative}$  then  $\triangleright$  switch gradient
16:       $\mathbf{g} \leftarrow -\hat{\mathbf{g}}$ 
17:    else
18:       $m_{rnd} \leftarrow$  randomly selected from  $\mathcal{M}$ 
19:       $\mathbf{g} \leftarrow \nabla_{\mathbf{x}_{adv}} \mathcal{L}(m_{rnd}(\mathbf{x}_{adv}), t)$ 
20:    end if
21:  end if
22:   $\mathbf{x}_{adv} \leftarrow \prod_{\mathcal{B}_2(\mathbf{x}, \epsilon)}(\mathbf{x}_{adv} + \eta \cdot \frac{\mathbf{g}}{\|\mathbf{g}\|_2})$   $\triangleright$  replacing this line
with  $\mathbf{x}_{adv} \leftarrow \prod_{\mathcal{B}_\infty(\mathbf{x}, \epsilon)}(\mathbf{x}_{adv} + \eta \cdot \text{sign}(\mathbf{g}))$  for  $\ell_\infty$  norm
attack, and  $\prod_{\mathcal{B}_p(\mathbf{x}, \epsilon)}$  means the  $\ell_p$  norm projection.
23:   $\mathbf{x}_{adv} \leftarrow \text{Clip}(\mathbf{x}_{adv}, 0, 1)$ 
24:   $L_{last} \leftarrow \mathcal{L}(f(\mathbf{x}_{adv}), t)$ 
25: end while
26: return  $\mathbf{x}_{adv}$ 

```

and Zhang 2019). After randomly selecting another surrogate model m_{rnd} from this set, SWITCH_{rnd} calculates the gradient $\nabla_{\mathbf{x}_{adv}} \mathcal{L}(m_{rnd}(\mathbf{x}_{adv}), t)$ to update the image \mathbf{x}_{adv} , the following steps are the same as SWITCH_{neg}, *i.e.*, image projection & record L_{last} . Experimental results in Tab. 2 validate that switching to the gradient of another model when necessary helps the optimization.

Experiment

Experiment Setting

Datasets and Target Models. Three datasets, namely, CIFAR-10 (Krizhevsky 2009), CIFAR-100 (Krizhevsky 2009), and TinyImageNet (Russakovsky et al. 2015), are used for the experiments. We randomly select 1,000 tested images from their validation sets for evaluation, all of which are correctly classified by Inception-v3 (Szegedy et al. 2016). In the CIFAR-10 and CIFAR-100 datasets,

we follow Yan *et al.* (Yan, Guo, and Zhang 2019) to select the following target models: (1) a 272-layer PyramidNet+Shakedrop model (PyramidNet-272) (Han, Kim, and Kim 2017; Yamada et al. 2018), which is the state-of-the-art network on CIFAR-10; (2) a model obtained through a neural architecture search called GDAS (Dong and Yang 2019); (3) a wide residual network with 28 layers and 10 times width expansion (WRN-28) (Zagoruyko and Komodakis 2016); and (4) a wide residual network with 40 layers and 10 times width expansion (WRN-40) (Zagoruyko and Komodakis 2016). In the TinyImageNet dataset, we select (1) ResNeXt-101 (32x4d) (Xie et al. 2016), (2) ResNeXt-101 (64x4d) (Xie et al. 2016), and (3) DenseNet-121 with a growth rate of 32 (Huang et al. 2017) as the target models.

Method Setting. Learning rate η is set to 2.0 for untargeted and targeted attacks under the ℓ_2 norm constraint, except for the targeted attack of CIFAR-100 dataset, which is set to 0.5. For the ℓ_∞ norm attack, we set η to 0.01. The ϵ is set to 4.6 in the ℓ_2 norm attack and 8/255 in the ℓ_∞ norm attack. Surrogate model m is selected as ResNet-110 in the CIFAR-10 & CIFAR-100 datasets and ResNet-101 in the TinyImageNet dataset. We select 13 models to constitute surrogate model set \mathcal{M} for the CIFAR-10 & CIFAR-100 datasets, and 15 models for the TinyImageNet dataset. The details of model set \mathcal{M} are presented in the appendix, which have different structures from the tested target models. Note that in the targeted attack, the target class is set to $y_{adv} = (y+1) \bmod C$ for all attacks, where y_{adv} is the target class, y is the true class, and C is the class number.

Compared Methods. The compared query-based black-box attacks are listed in Tab. 1. It includes Bandits attack (Ilyas, Engstrom, and Madry 2019), the nature evolution strategy (NES) (Ilyas et al. 2018b), Meta Attack (Du et al. 2020), RGF method (Nesterov 2017), P-RGF method (Cheng et al. 2019), Projection & Probability-driven Black-box Attack (PPBA) (Li et al. 2020), Parsimonious (Moon, An, and Song 2019), Simple Black-box Attacks (SimBA) (Guo et al. 2019), SignHunter (Al-Dujaili and O’Reilly 2019), and Square Attack (Andriushchenko et al. 2020). These methods consist of different strategies. Bandits, NES, RGF, and P-RGF estimate the approximate gradient to optimize the adversarial example; SimBA, PPBA, and Square Attack rely on random search optimization; Parsimonious optimizes a discrete surrogate problem by finding the solution among the vertices of the ℓ_∞ ball; PPBA utilizes a low-frequency constrained sensing matrix; P-RGF and Meta Attack require

Method	Surrogate Model(s)	Gradient Estimation	Based on Random Search
Bandits	×	✓	×
NES	×	✓	×
RGF	×	✓	×
P-RGF	✓	✓	×
Meta Attack	✓	✓	×
PPBA	×	×	✓
Parsimonious	×	×	×
SimBA	×	×	✓
SignHunter	×	×	×
Square Attack	×	×	✓
SWITCH	✓	×	×

Table 1: Different attack methods adopt different strategies.

Attack	switch ratio			$L_{\text{switched}} > L_{\text{last}}$ ratio			$L_{\text{switched}} > L_{\mathbf{x}_{\text{temp}}}$ ratio		
	D ₁₂₁	R ₃₂	R ₆₄	D ₁₂₁	R ₃₂	R ₆₄	D ₁₂₁	R ₃₂	R ₆₄
SWITCH _{neg}	43.9%	43.9%	46.1%	45%	48.6%	44.3%	70%	73.1%	69.5%
SWITCH _{rnd}	36.8%	36.6%	45.1%	74.5%	86.5%	67.6%	90.1%	94.5%	86.3%
SWITCH _{neg}	41.4%	40.8%	40.4%	50.3%	52.5%	53.3%	72.3%	74.1%	74.1%
SWITCH _{rnd}	44.6%	42.9%	44.9%	76.3%	78.9%	77.9%	90%	92%	91.2%

Table 2: The ratio of performing switch operation and the corresponding increased loss in all iterations of attacking 1,000 TinyImageNet tested images. The first row block shows ℓ_2 norm untargeted attack, and the second row block shows ℓ_∞ norm untargeted attack. D₁₂₁: DenseNet-121, R₃₂: ResNeXt-101 (32×4d), R₆₄: ResNeXt-101 (64×4d).

surrogate models. Tab. 1 summarizes the strategies of these methods. We use the PyTorch (Paszke et al. 2019) framework for all experiments, and the official PyTorch implementations of Meta Attack, PPBA, Bandits, SimBA, Sign-Hunter, and Square Attack are used in the experiments. For experimental consistency, we translate the code of NES, Parsimonious, RGF, and P-RGF from the official TensorFlow (Abadi et al. 2016) implementation into the PyTorch version. The official implementations of RGF and P-RGF only support untargeted attack, so they are excluded from the targeted attack experiments. Parsimonious only supports ℓ_∞ norm attack. P-RGF improves query efficiency of RGF by utilizing surrogate models, and uses the same surrogate model m as our method does. All methods are limited to a maximum of 10,000 queries in all experiments. The same ϵ value is set for all attacks, that is, 4.6 in the ℓ_2 norm attack and 8/255 in the ℓ_∞ norm attack. The configurations of these methods are provided in the appendix.

Evaluation Metric. According to previous studies (Ilyas et al. 2018a; Yan, Guo, and Zhang 2019), we use the attack success rate, the average and the median of queries as the evaluation metric. All attacks are performed on the correctly classified benign images, so the attack success rate is calculated based on them. The average and median of queries are counted on the successful attacked images.

Ablation Study

The Ratio of Increased Loss with SWITCH. To inspect the effectiveness of SWITCH, we conduct one-step empirical analysis on TinyImageNet with untargeted attack, *i.e.*, we check whether the loss could be increased or decreased by following the switched gradients. Specifically, we first count the proportion of switch operations performed in all attack iterations. Then, only the samples that are updated by using the switched gradient are selected and then sent to the target model to record a loss L_{switched} . The ratio of samples with L_{switched} larger than the loss of previous iteration (L_{last}) is counted ($L_{\text{switched}} > L_{\text{last}}$ ratio). The ratio of $L_{\text{switched}} > L_{\mathbf{x}_{\text{temp}}}$ is counted to check whether the switched gradient is better than the gradient before switching, where \mathbf{x}_{temp} is the image updated by using the surrogate gradient before switching. Results of Tab. 2 show that (1) switching is better than not switching (see $L_{\text{switched}} > L_{\mathbf{x}_{\text{temp}}}$ ratio); (2) switching gradients are rather effective in optimization, since the losses of a large fraction of samples are increased

Attack	Attack Success Rate			Avg. Query			Median Query		
	D ₁₂₁	R ₃₂	R ₆₄	D ₁₂₁	R ₃₂	R ₆₄	D ₁₂₁	R ₃₂	R ₆₄
NO SWITCH	96.9%	96.5%	94.5%	119	110	183	4	5	5
SWITCH _{neg}	99.6%	99.6%	98.8%	30	19	24	3	4	4
SWITCH _{rnd}	100%	99.9%	99.9%	5	6	21	3	4	3
NO SWITCH	50.1%	35%	33.9%	685	866	878	31	40	44
SWITCH _{neg}	86.8%	75.5%	73%	322	611	503	20	37	37
SWITCH _{rnd}	94.4%	87.7%	88.1%	167	265	269	11	17	17

Table 3: NO SWITCH vs. SWITCH_{neg} vs. SWITCH_{rnd} of untargeted attack experiments on TinyImageNet dataset. The first row block shows ℓ_2 norm attack, and the second row block shows ℓ_∞ norm attack. D₁₂₁: DenseNet-121, R₃₂: ResNeXt-101 (32×4d), R₆₄: ResNeXt-101 (64×4d).

from the last iteration after following the switched gradient ($L_{\text{switched}} > L_{\text{last}}$) even though they have $L_{\mathbf{x}_{\text{temp}}} < L_{\text{last}}$.

NO SWITCH versus SWITCH. To validate the effectiveness of the gradient switch operation in terms of attack success rate and query efficiency, we compare SWITCH_{rnd} and SWITCH_{neg} with NO SWITCH, *i.e.*, the algorithm without switching the surrogate gradient. In other words, NO SWITCH directly uses the gradient \hat{g} of the surrogate model m , which is not changed during the attack. The experimental results on TinyImageNet are listed in Tab. 3. We can draw the following conclusions based on Tab. 3:

- (1) NO SWITCH performs the worst among all variants. Thus, the switching of the gradient direction is crucial for achieving high attack success rate and query efficiency.
- (2) SWITCH_{rnd} outperforms SWITCH_{neg} with fewer queries and higher attack success rate. This result is consistent with Tab. 2 which shows that SWITCH_{rnd} can increase the loss L_{switched} more than SWITCH_{neg}.

Comparisons with State-of-the-Art Methods

Untargeted and Targeted Attack Results. We compare the proposed approach with state-of-the-art methods by attacking PyramidNet-272, GDAS, WRN-28, and WRN-40 in CIFAR-10 & CIFAR-100 datasets. Tab. 4 and Tab. 5 show the experimental results of the untargeted and targeted attack on CIFAR-10 & CIFAR-100 datasets. In TinyImageNet, we conduct experiments by attacking DenseNet-121, ResNeXt-101 (32×4d), and ResNeXt-101 (64×4d), whose results are shown in Tab. 6, Tab. 7 and Tab. 8. RGF and P-RGF are excluded from the targeted attack experiments because their official implementations only support the untargeted attack. These results demonstrate that (1) the performance of SWITCH_{neg} is already satisfactory for untargeted attack in CIFAR-10 & CIFAR-100. Tab. 4 shows that SWITCH_{neg} requires only a few queries (≤ 3) to achieve 100% success rate in ℓ_2 norm attack; (2) SWITCH_{rnd} performs the best among all attack methods. To inspect the performance of attacking defensive models, we conduct the experiments of attacking two defensive models, *i.e.*, ComDefend (Jia et al. 2019) and Feature Distillation (Liu et al. 2019), and the results are presented in the appendix due to space limitation.

Detailed Experimental Figures. To present the results more comprehensively, we investigate the attack success

Dataset	Norm	Attack	Attack Success Rate				Avg. Query				Median Query			
			PyramidNet-272	GDAS	WRN-28	WRN-40	PyramidNet-272	GDAS	WRN-28	WRN-40	PyramidNet-272	GDAS	WRN-28	WRN-40
CIFAR-10	ℓ_2	NES	99.3%	74.8%	99.9%	99.5%	202	123	159	154	200	100	100	100
		RGF	100%	100%	100%	100%	216	168	153	150	204	152	102	152
		P-RGF	100%	100%	100%	100%	64	40	76	73	62	20	64	64
		Meta Attack	84.2%	92.9%	92.4%	95.1%	3410	2097	2202	1996	2862	1561	1562	1433
		Bandits	100%	100%	100%	100%	151	66	107	98	110	54	80	78
		PPBA	99%	100%	100%	99.9%	181	130	146	127	110	63	86	83
		SimBA	99.9%	96.4%	99.7%	99.8%	331	357	292	261	243	142	187	192
		SignHunter	100%	99%	100%	100%	103	91	93	74	54	28	40	36
		Square Attack	100%	100%	100%	100%	46	16	24	24	26	4	7	7
		SWITCH _{neg}	100%	100%	100%	100%	3	2	2	2	2	2	2	2
		SWITCH _{rnd}	100%	100%	100%	100%	2	2	2	2	2	2	2	2
		CIFAR-100	ℓ_∞	NES	86.8%	71.4%	74.2%	77.6%	1559	628	1235	1209	600	300
RGF	99%			93.8%	98.6%	98.8%	955	646	1178	928	668	460	663	612
P-RGF	97.3%			97.9%	97.7%	98%	742	337	703	564	408	128	236	217
Meta Attack	33.8%			61.7%	64%	71.7%	3668	3055	2658	2566	2864	2344	1950	1823
Bandits	99.6%			100%	99.4%	99.9%	1015	391	611	542	560	166	224	228
PPBA	96.6%			99.4%	96.8%	97.4%	860	327	714	533	322	120	196	179
Parsimonious	100%			100%	100%	100%	701	345	891	738	523	230	424	375
SimBA	93.9%			94.9%	93.8%	96.1%	743	504	715	677	387	205	316	331
SignHunter	99.4%			91.8%	100%	100%	379	253	506	415	189	106	205	188
Square Attack	100%			100%	99.9%	100%	332	126	403	342	182	54	144	139
SWITCH _{neg}	78.7%			96.8%	97.1%	97.6%	441	111	85	89	23	4	3	3
SWITCH _{rnd}	87.9%			98.3%	98.5%	98.7%	203	45	36	40	9	4	3	3
CIFAR-100	ℓ_2	NES	92.5%	90.1%	98.3%	99.7%	118	83	103	106	100	50	100	100
		RGF	100%	100%	100%	100%	114	110	106	106	102	101	102	102
		P-RGF	100%	100%	100%	100%	54	46	54	73	62	62	62	62
		Meta Attack	99.1%	99.7%	99.7%	98.3%	850	798	1098	1163	651	524	781	782
		Bandits	100%	100%	100%	100%	58	54	64	65	42	42	52	52
		PPBA	99.6%	99.9%	99.6%	99.9%	74	67	94	100	39	35	46	48
		SimBA	100%	98.1%	99.8%	99.6%	172	157	176	202	96	56	104	108
		SignHunter	100%	99.9%	100%	100%	32	26	38	44	16	10	16	14
		Square Attack	100%	100%	100%	100%	8	5	10	9	1	1	1	1
		SWITCH _{neg}	100%	100%	100%	100%	2	1	2	2	1	1	1	1
		SWITCH _{rnd}	100%	100%	100%	100%	2	1	2	2	1	1	1	1
		CIFAR-100	ℓ_∞	NES	91.3%	89.7%	92.5%	89.5%	430	266	660	606	200	150
RGF	99.7%			98.8%	98.9%	99%	385	420	544	628	256	255	357	357
P-RGF	99.3%			98.3%	98%	97.8%	308	220	371	480	147	116	136	181
Meta Attack	99.7%			99.5%	98.3%	97.1%	932	922	1142	1226	653	652	782	782
Bandits	100%			100%	99.8%	99.8%	266	209	262	260	68	56	106	92
PPBA	99.3%			99.8%	98.8%	98.6%	164	157	275	279	63	49	82	77
Parsimonious	100%			100%	100%	99.9%	287	185	383	422	204	103	215	213
SimBA	99.9%			97.8%	98.2%	97%	322	190	386	431	127	67	150	152
SignHunter	99%			97.3%	99.8%	100%	125	119	211	255	52	37	59	60
Square Attack	100%			100%	100%	99.8%	76	57	150	162	17	19	46	36
SWITCH _{neg}	92.9%			96.8%	94.1%	94.6%	108	41	120	90	4	3	3	3
SWITCH _{rnd}	96.9%			97.1%	95.3%	96.6%	69	50	77	57	4	3	3	3

Table 4: Experimental results of untargeted attack in CIFAR-10 and CIFAR-100 datasets.

Dataset	Attack	Attack Success Rate				Avg. Query				Median Query			
		PyramidNet-272	GDAS	WRN-28	WRN-40	PyramidNet-272	GDAS	WRN-28	WRN-40	PyramidNet-272	GDAS	WRN-28	WRN-40
CIFAR-10	NES	93.7%	95.3%	98.5%	97.7%	1474	1515	1043	1088	1251	999	881	882
	Meta Attack	35.2%	70.9%	55.1%	56.4%	4584	3809	4131	4097	4352	3328	3586	3714
	Bandits	99.7%	100%	97.3%	98.4%	852	718	1082	997	458	538	338	398
	PPBA	98.8%	99.8%	97.1%	99.4%	696	444	740	612	307	220	284	269
	SimBA	99.2%	99.7%	98.5%	99.2%	588	358	537	418	455	274	394	359
	SignHunter	100%	100%	100%	100%	336	131	247	177	200	78	126	102
	Square Attack	100%	100%	100%	100%	142	94	124	96	89	62	61	56
	SWITCH _{neg}	99.3%	93.2%	99.8%	100%	171	395	120	27	9	11	5	5
	SWITCH _{rnd}	100%	100%	100%	100%	6	7	4	4	5	5	4	4
	CIFAR-100	NES	87.6%	77%	89.3%	87.5%	1300	1405	1383	1424	1102	1172	1061
Meta Attack		85%	89.1%	63.2%	42.3%	3833	3521	4713	4861	3457	2946	4481	4610
Bandits		99.6%	100%	98.9%	91.5%	1442	847	1645	2436	1056	678	1150	1578
PPBA		98.8%	99.8%	98.3%	92.9%	803	476	907	1546	434	306	469	742
SimBA		99.2%	99.7%	97.8%	94.7%	522	358	590	658	403	289	446	539
SignHunter		100%	100%	100%	100%	371	269	385	441	267	149	226	260
Square Attack		100%	100%	100%	99.8%	250	175	262	384	151	121	163	178
SWITCH _{neg}		86.8%	86.4%	86.4%	78.8%	801	723	985	1089	145	86	159	202
SWITCH _{rnd}		100%	100%	100%	100%	26	31	26	27	16	16	15	16

Table 5: Experimental results of targeted attack under ℓ_2 norm constraint in CIFAR-10 and CIFAR-100 datasets.

Attack	Attack Success Rate			Avg. Query			Median Query		
	D ₁₂₁	R ₃₂	R ₆₄	D ₁₂₁	R ₃₂	R ₆₄	D ₁₂₁	R ₃₂	R ₆₄
NES	85.4%	68.5%	68.2%	334	507	545	250	350	350
RGF	99.4%	98.7%	98.9%	364	741	679	255	410	410
P-RGF	99.8%	99.3%	99.1%	217	270	285	84	86	85
Meta Attack	91.1%	85.3%	86.4%	3596	4053	4105	3074	3585	3712
Bandits	100%	99.5%	99.7%	421	823	774	256	456	458
PPBA	99.8%	99.8%	99.6%	231	481	412	146	251	243
SimBA	98%	92.9%	93.7%	278	489	482	186	341	333
SignHunter	99.6%	99.5%	99.9%	119	334	322	37	61	75
Square Attack	100%	99.5%	99.9%	85	224	230	28	58	53
SWITCH _{neg}	99.6%	99.6%	98.8%	30	19	24	3	4	4
SWITCH _{rnd}	100%	99.9%	99.9%	5	6	21	3	4	3

Table 6: Experimental results of untargeted attack under ℓ_2 norm in TinyImageNet dataset. D₁₂₁: DenseNet-121, R₃₂: ResNeXt-101 (32×4d), R₆₄: ResNeXt-101 (64×4d).

Attack	Attack Success Rate			Avg. Query			Median Query		
	D ₁₂₁	R ₃₂	R ₆₄	D ₁₂₁	R ₃₂	R ₆₄	D ₁₂₁	R ₃₂	R ₆₄
NES	74.6%	45.4%	45.4%	1358	2038	2038	500	800	800
RGF	96.4%	85.3%	87.5%	1146	2088	2097	667	1280	1326
P-RGF	94.5%	83.9%	85.9%	883	1583	1581	448	657	690
Meta Attack	71.6%	36%	37.4%	3973	3979	4109	3329	3585	3457
Bandits	99.2%	94.1%	95.3%	964	1737	1662	520	954	1014
PPBA	99.6%	97.9%	98.2%	403	926	814	191	404	389
Parsimonious	100%	99.3%	99.3%	273	643	579	190	300	284
SimBA	98.1%	93.8%	94.6%	381	861	855	197	410	391
SignHunter	99.5%	98.6%	99%	201	581	527	59	122	152
Square Attack	100%	99.4%	99.6%	160	396	379	74	158	142
SWITCH _{neg}	86.8%	75.5%	73%	322	611	503	20	37	37
SWITCH _{rnd}	94.4%	87.7%	88.1%	167	265	269	11	17	17

Table 7: Experimental results of untargeted attack under ℓ_∞ norm in TinyImageNet dataset. D₁₂₁: DenseNet-121, R₃₂: ResNeXt-101 (32×4d), R₆₄: ResNeXt-101 (64×4d).

Attack	Attack Success Rate			Avg. Query			Median Query		
	D ₁₂₁	R ₃₂	R ₆₄	D ₁₂₁	R ₃₂	R ₆₄	D ₁₂₁	R ₃₂	R ₆₄
NES	88.5%	88%	88.2%	4625	4959	4758	4337	4702	4440
Meta Attack	23.7%	20.7%	17.9%	5351	5537	5601	5250	5249	5248
Bandits	85.1%	72.2%	72.4%	2724	3550	3542	1860	2698	2852
PPBA	89.3%	85.4%	83.7%	1593	2321	2153	901	1388	1383
SimBA	85.6%	59.8%	66.8%	933	901	946	740	809	865
SignHunter	97.9%	96.9%	98%	1127	1624	1597	649	995	992
Square Attack	96.6%	94%	94.7%	1014	1649	1628	455	836	759
SWITCH _{neg}	59.1%	56.2%	51.7%	1302	1312	1310	321	275	294
SWITCH _{rnd}	94.7%	93.9%	94%	179	186	286	28	29	30

Table 8: Experimental results of targeted attack under ℓ_2 norm in TinyImageNet dataset. D₁₂₁: DenseNet-121, R₃₂: ResNeXt-101 (32×4d), R₆₄: ResNeXt-101 (64×4d).

rates by limiting different maximum numbers of queries in targeted attacks under ℓ_2 norm constraint. Fig. 3 shows the superior success rate of the proposed approach. Fig. 4 demonstrates the relation between the query number and the attack success rate from a different angle. Fig. 4 shows the average query number that reaches different desired success rates. Specifically, given a desired success rate a and the query list Q of all samples, the average query (Avg. Q_a) is defined as follows:

$$\text{Avg. } Q_a = \frac{\sum_{i=1}^N \hat{Q}_i}{N}, \quad \text{where } \hat{Q} = Q[Q \leq P_a], \quad (2)$$

where P_a is the a th percentile value of Q and N is the length

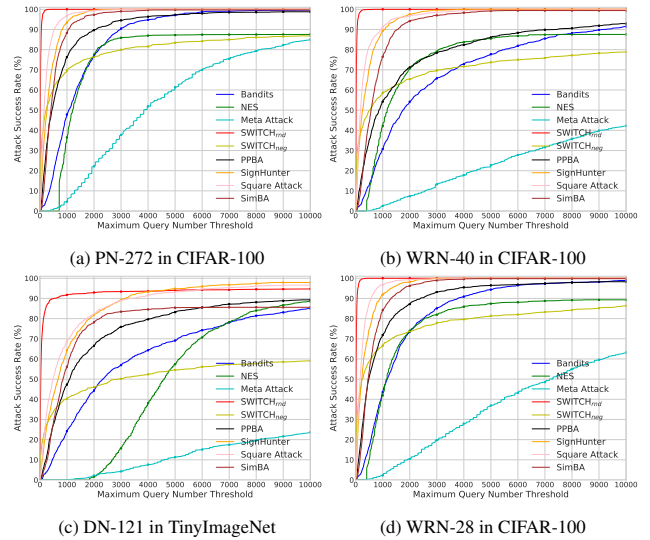


Figure 3: Comparison of attack success rate at different limited maximum queries in targeted attack under ℓ_2 norm, where PN-272: PyramidNet-272, DN-121: DenseNet-121.

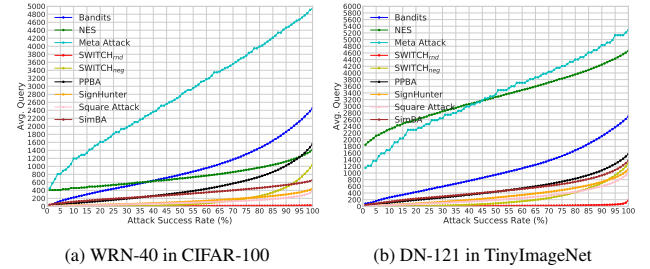


Figure 4: Comparison of the average query per successful image at different desired success rates in the targeted attack under ℓ_2 norm, where DN-121 is DenseNet-121.

of \hat{Q} . Fig. 4 shows that SWITCH_{rnd} produces the lowest curve and is significantly more query-efficient than others. More figures are presented in the appendix.

Conclusion

In this study, we propose a simple and highly efficient black-box attack named SWITCH. SWITCH exploits the gradient of a surrogate model and then switches the gradient if it points to the non-adversarial region of target model, which keeps the loss function increasing as much as possible. Two switch operations are introduced, *i.e.*, SWITCH_{neg} and SWITCH_{rnd}, which adopt different strategies to determine a new direction. These strategies significantly boost the optimization process. Extensive experiments demonstrate that the proposed method achieves state-of-the-art performance.

Acknowledgments

This research was supported by the National Natural Science Foundation of China (Grant Nos. 61972221, 61572274, 61672307).

References

- Abadi, M.; Barham, P.; Chen, J.; Chen, Z.; Davis, A.; Dean, J.; Devin, M.; Ghemawat, S.; Irving, G.; Isard, M.; et al. 2016. Tensorflow: A system for large-scale machine learning. In *12th {USENIX} Symposium on Operating Systems Design and Implementation ({OSDI} 16)*, 265–283.
- Al-Dujaili, A.; and O’Reilly, U.-M. 2019. Sign Bits Are All You Need for Black-Box Attacks. In *International Conference on Learning Representations*.
- Andriushchenko, M.; Croce, F.; Flammarion, N.; and Hein, M. 2020. Square Attack: a query-efficient black-box adversarial attack via random search.
- Bhagoji, A. N.; He, W.; Li, B.; and Song, D. 2018. Practical black-box attacks on deep neural networks using efficient query mechanisms. In *European Conference on Computer Vision*, 158–174. Springer.
- Carlini, N.; and Wagner, D. A. 2017. Towards Evaluating the Robustness of Neural Networks. In *IEEE Symposium on Security and Privacy (SP)*, 39–57. ISSN 2375-1207. doi:10.1109/SP.2017.49.
- Chen, P.-Y.; Zhang, H.; Sharma, Y.; Yi, J.; and Hsieh, C.-J. 2017. Zoo: Zeroth order optimization based black-box attacks to deep neural networks without training substitute models. In *Proceedings of the 10th ACM Workshop on Artificial Intelligence and Security*, 15–26. ACM.
- Cheng, M.; Singh, S.; Chen, P.-Y.; Liu, S.; and Hsieh, C.-J. 2020. Sign-OPT: A Query-Efficient Hard-label Adversarial Attack URL <https://openreview.net/forum?id=SkITQCNTvS>.
- Cheng, S.; Dong, Y.; Pang, T.; Su, H.; and Zhu, J. 2019. Improving black-box adversarial attacks with a transfer-based prior. In *Advances in Neural Information Processing Systems*, 10932–10942.
- Demontis, A.; Melis, M.; Pintor, M.; Jagielski, M.; Biggio, B.; Oprea, A.; Nita-Rotaru, C.; and Roli, F. 2019. Why Do Adversarial Attacks Transfer? Explaining Transferability of Evasion and Poisoning Attacks. In *28th USENIX Security Symposium (USENIX Security 19)*, 321–338. Santa Clara, CA: USENIX Association. ISBN 978-1-939133-06-9. URL <https://www.usenix.org/conference/usenixsecurity19/presentation/demontis>.
- Dong, X.; and Yang, Y. 2019. Searching for a robust neural architecture in four gpu hours. In *Proceedings of the IEEE Conference on Computer Vision and Pattern Recognition*, 1761–1770.
- Dong, Y.; Su, H.; Wu, B.; Li, Z.; Liu, W.; Zhang, T.; and Zhu, J. 2019. Efficient decision-based black-box adversarial attacks on face recognition. In *Proceedings of the IEEE Conference on Computer Vision and Pattern Recognition*, 7714–7722.
- Du, J.; Zhang, H.; Zhou, J. T.; Yang, Y.; and Feng, J. 2020. Query-efficient Meta Attack to Deep Neural Networks. In *International Conference on Learning Representations*. URL <https://openreview.net/forum?id=Skxd6gSYDS>.
- Goodfellow, I. J.; Shlens, J.; and Szegedy, C. 2015. Explaining and Harnessing Adversarial Examples. In *3rd International Conference on Learning Representations*. URL <http://arxiv.org/abs/1412.6572>.
- Guo, C.; Gardner, J. R.; You, Y.; Wilson, A. G.; and Weinberger, K. Q. 2019. Simple black-box adversarial attacks. *arXiv preprint arXiv:1905.07121*.
- Han, D.; Kim, J.; and Kim, J. 2017. Deep pyramidal residual networks. In *Proceedings of the IEEE conference on computer vision and pattern recognition*, 5927–5935.
- Huang, G.; Liu, Z.; van der Maaten, L.; and Weinberger, K. Q. 2017. Densely Connected Convolutional Networks. In *The IEEE Conference on Computer Vision and Pattern Recognition (CVPR)*.
- Huang, Q.; Katsman, I.; He, H.; Gu, Z.; Belongie, S.; and Lim, S.-N. 2019. Enhancing adversarial example transferability with an intermediate level attack. In *Proceedings of the IEEE International Conference on Computer Vision*, 4733–4742.
- Huang, Z.; and Zhang, T. 2020. Black-Box Adversarial Attack with Transferable Model-based Embedding. In *International Conference on Learning Representations*. URL <https://openreview.net/forum?id=SJxhNTNYwB>.
- Ilyas, A.; Engstrom, L.; Athalye, A.; and Lin, J. 2018a. Black-box Adversarial Attacks with Limited Queries and Information. In *Proceedings of the 35th International Conference on Machine Learning, ICML 2018*. URL <https://arxiv.org/abs/1804.08598>.
- Ilyas, A.; Engstrom, L.; Athalye, A.; and Lin, J. 2018b. Black-box adversarial attacks with limited queries and information. *arXiv preprint arXiv:1804.08598*.
- Ilyas, A.; Engstrom, L.; and Madry, A. 2019. Prior Convictions: Black-box Adversarial Attacks with Bandits and Priors. In *International Conference on Learning Representations*. URL <https://openreview.net/forum?id=BkMiWhR5K7>.
- Inkawhich, N.; Wen, W.; Li, H. H.; and Chen, Y. 2019. Feature space perturbations yield more transferable adversarial examples. In *Proceedings of the IEEE Conference on Computer Vision and Pattern Recognition*, 7066–7074.
- Jia, X.; Wei, X.; Cao, X.; and Foroosh, H. 2019. Comdefend: An efficient image compression model to defend adversarial examples. In *Proceedings of the IEEE Conference on Computer Vision and Pattern Recognition*, 6084–6092.
- Krizhevsky, A. 2009. Learning multiple layers of features from tiny images. Technical report.
- Krizhevsky, A.; Hinton, G.; et al. 2009. Learning multiple layers of features from tiny images.
- Li, J.; Ji, R.; Liu, H.; Liu, J.; Zhong, B.; Deng, C.; and Tian, Q. 2020. Projection & Probability-Driven Black-Box Attack. In *Proceedings of the IEEE/CVF Conference on Computer Vision and Pattern Recognition*, 362–371.
- Liu, Y.; Chen, X.; Liu, C.; and Song, D. 2017. Delving into Transferable Adversarial Examples and Black-box Attacks. In *Proceedings of 5th International Conference on Learning Representations*.
- Liu, Z.; Liu, Q.; Liu, T.; Xu, N.; Lin, X.; Wang, Y.; and Wen, W. 2019. Feature distillation: Dnn-oriented jpeg compression against adversarial examples. In *2019 IEEE/CVF Conference on Computer Vision and Pattern Recognition (CVPR)*, 860–868. IEEE.
- Ma, C.; Chen, L.; and Yong, J. 2020. MetaSimulator: Simulating Unknown Target Models for Query-Efficient Black-box Attacks. *arXiv preprint arXiv:2009.00960*.
- Ma, C.; Zhao, C.; Shi, H.; Chen, L.; Yong, J.; and Zeng, D. 2019. MetaAdvDet: Towards Robust Detection of Evolving Adversarial Attacks. In *Proceedings of the 27th ACM International Conference on Multimedia*, MM 19, 692701. New York, NY, USA: Association for Computing Machinery. ISBN 9781450368896. doi:10.1145/3343031.3350887. URL <https://doi.org/10.1145/3343031.3350887>.
- Madry, A.; Makelov, A.; Schmidt, L.; Tsipras, D.; and Vladu, A. 2018. Towards Deep Learning Models Resistant to Adversarial Attacks. In *International Conference on Learning Representations*. URL <https://openreview.net/forum?id=rJzIBfZAb>.

- Moon, S.; An, G.; and Song, H. O. 2019. Parsimonious Black-Box Adversarial Attacks via Efficient Combinatorial Optimization. In *International Conference on Machine Learning (ICML)*.
- Nesterov, Y. 2017. Random gradient-free minimization of convex functions. *Foundations of Computational Mathematics* 17(2): 527–566.
- Papernot, N.; McDaniel, P.; and Goodfellow, I. 2016. Transferability in machine learning: from phenomena to black-box attacks using adversarial samples. *arXiv preprint arXiv:1605.07277*.
- Paszke, A.; Gross, S.; Massa, F.; Lerer, A.; Bradbury, J.; Chanan, G.; Killeen, T.; Lin, Z.; Gimelshein, N.; Antiga, L.; et al. 2019. PyTorch: An imperative style, high-performance deep learning library. In *Advances in Neural Information Processing Systems*, 8024–8035.
- Russakovsky, O.; Deng, J.; Su, H.; Krause, J.; Satheesh, S.; Ma, S.; Huang, Z.; Karpathy, A.; Khosla, A.; Bernstein, M.; et al. 2015. Imagenet large scale visual recognition challenge. *International journal of computer vision* 115(3): 211–252.
- Szegedy, C.; Vanhoucke, V.; Ioffe, S.; Shlens, J.; and Wojna, Z. 2016. Rethinking the inception architecture for computer vision. In *Proceedings of the IEEE conference on computer vision and pattern recognition*, 2818–2826.
- Tu, C.-C.; Ting, P.; Chen, P.-Y.; Liu, S.; Zhang, H.; Yi, J.; Hsieh, C.-J.; and Cheng, S.-M. 2019. Autozoom: Autoencoder-based zeroth order optimization method for attacking black-box neural networks. In *Proceedings of the AAAI Conference on Artificial Intelligence*, volume 33, 742–749.
- Xie, S.; Girshick, R.; Dollr, P.; Tu, Z.; and He, K. 2016. Aggregated Residual Transformations for Deep Neural Networks. *arXiv preprint arXiv:1611.05431*.
- Yamada, Y.; Iwamura, M.; Akiba, T.; and Kise, K. 2018. Shake-drop regularization for deep residual learning. *arXiv preprint arXiv:1802.02375*.
- Yan, Z.; Guo, Y.; and Zhang, C. 2019. Subspace Attack: Exploiting Promising Subspaces for Query-Efficient Black-box Attacks. In *Advances in Neural Information Processing Systems*, 3820–3829.
- Zagoruyko, S.; and Komodakis, N. 2016. Wide Residual Networks. In *BMVC*.

Appendix: Experiment Settings

Settings of Compared Methods

RGF and P-RGF attack. Hyperparameters of RGF (Nesterov 2017) and P-RGF (Cheng et al. 2019) attacks are listed in Tab. 10. The experiments of RGF and P-RGF are conducted by using the PyTorch version translated from the official TensorFlow implementation located in P-RGF’s Github repository.

Norm	Hyperparameter	Value
ℓ_2	h , image learning rate	2.0
	σ , sampling variance	1e-4
	ϵ , maximum radius of ℓ_2 norm ball	4.6
ℓ_∞	h , image learning rate	0.005
	σ , sampling variance	1e-4
	ϵ , maximum radius of ℓ_∞ norm ball	8/255
ℓ_2, ℓ_∞	surrogate model used in CIFAR-10/100	ResNet-110
ℓ_2, ℓ_∞	surrogate model used in TinyImageNet	ResNet-101

Table 9: The hyperparameters of RGF and P-RGF attacks.

Bandits. Hyperparameters of Bandits (Ilyas, Engstrom, and Madry 2019) are listed in Tab. 10. The OCO learning rate is used to update the prior, where the prior is an alias of gradient g for updating the input image.

Parsimonious. Hyperparameters of Parsimonious (Moon, An, and Song 2019) are listed in Tab. 11. Parsimonious only supports ℓ_∞ norm attack. We follow the official implementation to set the initial block size to 4 in all experiments.

SignHunter. Hyperparameters of SignHunter (Al-Dujaili and O’Reilly 2019) are listed in Tab. 12.

Square Attack. Hyperparameters of Square Attack (Andriushchenko et al. 2020) are shown in Tab. 13. Square Attack randomly samples a square window filled with perturbations in each iteration. The area of this square window in the first iteration is initialized as $H \times W \times p$, which is then reduced in subsequent iterations.

PPBA. Hyperparameters of Projection & Probability-driven Black-box Attack (PPBA) (Li et al. 2020) are shown in

Norm	Hyperparameter	Value
ℓ_2	δ , finite difference probe	0.01
	η , image learning rate	0.1
	η_g , OCO learning rate	0.1
	τ , Bandits exploration	0.3
	ϵ , maximum radius of ℓ_2 norm ball	4.6
	maximum query times	10,000
ℓ_∞	δ , finite difference probe	0.1
	η , image learning rate	1/255
	η_g , OCO learning rate	1.0
	τ , Bandits exploration	0.3
	ϵ , maximum radius of ℓ_∞ norm ball	8/255
	maximum query times	10,000

Table 10: The hyperparameters of Bandits.

Hyperparameter	Value
the number of iterations in local search	1
k , initial block size	4
batch size	64
no hierarchical evaluation	False
ϵ , maximum radius ℓ_∞ norm ball	8/255

Table 11: The hyperparameters of Parsimonious.

Hyperparameter	Value
ϵ , maximum radius of ℓ_2 norm ball	4.6
ϵ , maximum radius of ℓ_∞ norm ball	8/255

Table 12: The hyperparameters of SignHunter.

Hyperparameter	Value
p , initial probability of changing a coordinate	0.05
ϵ , maximum radius of ℓ_2 norm ball	4.6
ϵ , maximum radius of ℓ_∞ norm ball	8/255

Table 13: The hyperparameters of Square Attack.

Dataset	Hyperparameter	Value
CIFAR-10/100	order	strided
	ρ , the change of measurement vector z	0.01
	μ , the momentum of calculating effective probability	1
	frequency dim, used in initialize blocks	11
	low-frequency dimension	1,500
	stride, used in initialize blocks	7
	number of samples per iteration	1
	ϵ , maximum radius ℓ_2 norm ball	4.6
	ϵ , maximum radius ℓ_∞ norm ball	8/255
TinyImageNet	order	strided
	ρ , the change of measurement vector z	0.01
	μ , the momentum of calculating effective probability	1
	frequency dim, used in initialize block	15
	low-frequency dimension	1,500
	stride, used in initialize block	7
	number of samples per iteration	1
	ϵ , maximum radius of ℓ_2 norm ball	4.6
	ϵ , maximum radius of ℓ_∞ norm ball	8/255

Table 14: The hyperparameters of PPBA.

Dataset	Hyperparameter	Value
CIFAR-10/100	order	strided
	frequency dim, used in initialize blocks	11
	stride, used in initialize blocks	7
	ϵ , maximum radius of ℓ_2 norm ball	4.6
	ϵ , maximum radius of ℓ_∞ norm ball	8/255
	pixel ϵ , step size per pixel	0.2
TinyImageNet	DCT mode	True
	order	strided
	frequency dim, used in initialize blocks	15
	stride, used in initialize blocks	7
	ϵ , maximum radius of ℓ_2 norm ball	4.6
	ϵ , maximum radius of ℓ_∞ norm ball	8/255
pixel ϵ , step size per pixel	0.2	
DCT mode	True	

Table 15: The hyperparameters of SimBA.

Tab. 14. We follow the official implementation to initialize the random matrix (strided) with the dimension of 1,500.

SimBA. Hyperparameters of Simple Black-box Attacks (SimBA) (Guo et al. 2019) are shown in Tab. 15. SimBA uses “strided mode” to construct perturbations during attack.

NES. Hyperparameters for NES attack (Ilyas et al. 2018b) are listed in Tab. 17. In the targeted attack setting, NES uses a randomly selected image of the target class as the initial image to optimize. Then, NES reduces its distance to the benign input image iteratively. Finally, the ℓ_p distance between the adversarial image and the benign image is within a preset ϵ . So, its hyperparameters are carefully tuned in untargeted and targeted attack separately, so as to achieve the highest attack success rate. The experiments of NES are conducted by using the PyTorch implementation.

Meta Attack. Hyperparameters of Meta Attack (Du et al. 2020) are listed in Tab. 18. the meta interval m is set to 3 in two cases, namely, the targeted attack and the experiments of TinyImageNet dataset. In other cases, the meta interval m is set to 5. The gradients of training data that are generated by using the pre-trained models listed in Tab. 19.

SWITCH. Hyperparameters of the proposed SWITCH are listed in Tab. 16. The configurations of the surrogate model

Norm	Hyperparameter	Value
ℓ_2	η , image learning rate except the ℓ_2 norm targeted attack on CIFAR-100	2.0
	η , image learning rate for the targeted attack under ℓ_2 norm on CIFAR-100	0.5
	ϵ , maximum radius of ℓ_2 norm ball	4.6
	ϵ , maximum radius of ℓ_∞ norm ball	8/255
ℓ_∞	η , image learning rate	0.01
	ϵ , maximum radius of ℓ_2 norm ball	8/255
ℓ_2, ℓ_∞	m , surrogate model used in CIFAR-10 & CIFAR-100 dataset	ResNet-110
ℓ_2, ℓ_∞	m , surrogate model used in TinyImageNet dataset	ResNet-101

Table 16: The hyperparameters of SWITCH attack.

Dataset	Attack	Norm	Hyperparameter	Value
CIFAR-10	Untargeted	ℓ_2	ϵ , radius of ℓ_2 norm ball	4.6
			h , learning rate	2.0
		ℓ_∞	ϵ , radius of ℓ_∞ norm ball	8/255
			h , learning rate	1e-2
	Targeted	ℓ_2	ϵ_0 , initial distance from the source image	20.0
			ϵ , final radius of ℓ_2 norm ball	4.6
			δ_{ϵ_0} , initial rate of decaying ϵ	1.0
			$\delta_{\epsilon_{\min}}$, the minimum rate of decaying ϵ	0.1
			ϵ	4.6
			h_{\max} , the maximum learning rate	2.0
	h_{\min} , the minimum learning rate	5e-5		
		ℓ_∞	ϵ_0 , initial distance from the source image	1.0
ϵ , final radius of ℓ_∞ norm ball			8/255	
δ_{ϵ_0} , initial rate of decaying ϵ			0.1	
$\delta_{\epsilon_{\min}}$, the minimum rate of decaying ϵ			0.01	
ϵ			0.1	
h_{\max} , the maximum learning rate			0.1	
h_{\min} , the minimum learning rate	0.01			
CIFAR-100	Untargeted	ℓ_2	ϵ , radius of ℓ_2 norm ball	4.6
			h , learning rate	2.0
		ℓ_∞	ϵ , radius of ℓ_∞ norm ball	8/255
			h , learning rate	1e-2
	Targeted	ℓ_2	ϵ_0 , initial distance from the source image	20.0
			ϵ , final radius of ℓ_2 norm ball	4.6
			δ_{ϵ_0} , initial rate of decaying ϵ	1.0
			$\delta_{\epsilon_{\min}}$, the minimum rate of decaying ϵ	0.3
			ϵ	1.0
			h_{\max} , the maximum learning rate	1.0
	h_{\min} , the minimum learning rate	5e-5		
		ℓ_∞	ϵ_0 , initial distance from the source image	1.0
ϵ , final radius of ℓ_∞ norm ball			8/255	
δ_{ϵ_0} , initial rate of decaying ϵ			0.1	
$\delta_{\epsilon_{\min}}$, the minimum rate of decaying ϵ			0.01	
ϵ			0.1	
h_{\max} , the maximum learning rate			0.1	
h_{\min} , the minimum learning rate	0.01			
TinyImageNet	Untargeted	ℓ_2	ϵ , radius of ℓ_2 norm ball	4.6
			h , learning rate	2.0
		ℓ_∞	ϵ , radius of ℓ_∞ norm ball	8/255
			h , learning rate	1e-2
	Targeted	ℓ_2	ϵ_0 , initial distance from the source image	40.0
			ϵ , final radius of ℓ_2 norm ball	4.6
			δ_{ϵ_0} , initial rate of decaying ϵ	1.0
			$\delta_{\epsilon_{\min}}$, the minimum rate of decaying ϵ	0.1
			ϵ	2.0
			h_{\max} , the maximum learning rate	2.0
	h_{\min} , the minimum learning rate	0.5		
		ℓ_∞	ϵ_0 , initial distance from the source image	1.0
ϵ , final radius of ℓ_∞ norm ball			8/255	
δ_{ϵ_0} , initial rate of decaying ϵ			0.1	
$\delta_{\epsilon_{\min}}$, the minimum rate of decaying ϵ			1e-3	
ϵ			0.1	
h_{\max} , the maximum learning rate			0.1	
h_{\min} , the minimum learning rate	0.01			

Table 17: The hyperparameters of NES attack, where the sampling variance σ for gradient estimation is set to 1e-3, the number of samples per draw is set to 50, and the maximum queries is set to 10,000 for all types of attacks in all datasets.

set \mathcal{M} used in SWITCH_{rnd} are listed in Tab. 19.

Pre-trained Networks and Target Models

Surrogate Model Set \mathcal{M} . In our experiments, 14 types of networks and 15 types of networks are selected as the surrogate model set \mathcal{M} in CIFAR-10/CIFAR-100 and TinyImageNet datasets, respectively. The names of these networks and their training configurations are shown in Tab. 19.

Additional Experiment Results

Results of Attacks on Defensive Models. Tab. 20 shows the experimental results of attacking defensive models. ComDefend (Jia et al. 2019) is a defensive model that consists of a compression convolutional neural network (ComCNN) and a reconstruction convolutional neural network (RecCNN) to transform the adversarial image into its clean version to defend against attacks. Feature Distillation (Liu et al. 2019) is a JPEG-based compression defensive framework. Both defensive models adopt the backbone as the ResNet-50 network. The results of Tab. 20 conclude that (1) SWITCH_{rnd} spends the fewest queries in breaking ComDefend and Feature Distillation on TinyImageNet dataset. (2) Parsimonious performs the best in breaking Feature Distillation on CIFAR-10 and CIFAR-100 datasets.

Detailed Experimental Figures. Fig. 5, Fig. 6, Fig. 7, Fig. 8, and Fig. 9 show the attack success rates by limiting different maximum queries. Fig. 10, Fig. 11, and Fig. 12 measure the average number of queries over successful images that reaches different desired success rates. These figures demonstrate the relation between the query number and the attack success rate from the different angle. Fig. 13, Fig. 14, Fig. 15 show the query number’s histogram of attacks on CIFAR-10, CIFAR-100, TinyImageNet. The results show that the highest red bars (SWITCH_{rnd}) are always located in the low query number’s area, thereby confirming that most adversarial examples of SWITCH_{rnd} have the fewest queries.

Dataset	Attack	Norm	Hyperparameter	Value
CIFAR-10/100	Untargeted	ℓ_2	h , learning rate top- q coordinates for estimating gradient m , meta interval use_tanh, the change-of-variables method ϵ , radius of ℓ_2 norm ball	1e-2 125 5 true 4.6
		ℓ_∞	h , learning rate top- q coordinates for estimating gradient m , meta interval use_tanh, the change-of-variables method ϵ , radius of ℓ_∞ norm ball	1e-2 125 5 false 8/255
	Targeted	ℓ_2	h , learning rate top- q coordinates for estimating gradient m , meta interval use_tanh, the change-of-variables method ϵ , radius of ℓ_2 norm ball	1e-2 125 3 true 4.6
		ℓ_∞	h , learning rate top- q coordinates for estimating gradient m , meta interval use_tanh, the change-of-variables method ϵ , radius of ℓ_∞ norm ball	1e-2 125 3 false 8/255
TinyImageNet	Untargeted	ℓ_2	h , learning rate top- q coordinates for estimating gradient m , meta interval use_tanh, the change-of-variables method ϵ , radius of ℓ_2 norm ball	1e-2 125 3 true 4.6
		ℓ_∞	h , learning rate top- q coordinates for estimating gradient m , meta interval use_tanh, the change-of-variables method ϵ , radius of ℓ_∞ norm ball	1e-2 125 3 false 8/255
	Targeted	ℓ_2	h , learning rate top- q coordinates for estimating gradient m , meta interval use_tanh, the change-of-variables method ϵ , radius of ℓ_2 norm ball	1e-2 125 3 true 4.6
		ℓ_∞	h , learning rate top- q coordinates for estimating gradient m , meta interval use_tanh, the change-of-variables method ϵ , radius of ℓ_∞ norm ball	1e-2 125 3 false 8/255

Table 18: The hyperparameters of Meta Attack, where the binary steps is set to 1, and the solver of gradient estimation adopts the adam for all types of attacks in all datasets.

Dataset	Network	Training Configuration					Hyperparameters	
		epochs	lr	lr decay epochs	lr decay rate	weight decay	layer depth	other hyperparameters
CIFAR-10/100	AlexNet	164	0.1	81, 122	0.1	5e-4	9	-
	DenseNet-100	300	0.1	150, 225	0.1	1e-4	100	growth rate:12, compression rate:2
	DenseNet-190	300	0.1	150, 225	0.1	1e-4	190	growth rate:40, compression rate:2
	PreResNet-110	164	0.1	81, 122	0.1	1e-4	110	block name: BasicBlock
	ResNeXt-29 (8 × 64d)	300	0.1	150, 225	0.1	5e-4	29	widen factor:4, cardinality:8
	ResNeXt-29 (16 × 64d)	300	0.1	150, 225	0.1	5e-4	29	widen factor:4, cardinality:16
	VGG-19 (BN)	164	0.1	81, 122	0.1	5e-4	19	-
	ResNet-20	164	0.1	81, 122	0.1	1e-4	20	block name: BasicBlock
	ResNet-32	164	0.1	81, 122	0.1	1e-4	32	block name: BasicBlock
	ResNet-44	164	0.1	81, 122	0.1	1e-4	44	block name: BasicBlock
	ResNet-50	164	0.1	81, 122	0.1	1e-4	50	block name: BasicBlock
	ResNet-56	164	0.1	81, 122	0.1	1e-4	56	block name: BasicBlock
	ResNet-110	164	0.1	81, 122	0.1	1e-4	110	block name: BasicBlock
ResNet-1202	164	0.1	81, 122	0.1	1e-4	1202	block name: BasicBlock	
TinyImageNet	VGG-11	300	1e-3	100, 200	0.1	1e-4	11	-
	VGG-11 (BN)	300	1e-3	100, 200	0.1	1e-4	11	-
	VGG-13	300	1e-3	100, 200	0.1	1e-4	13	-
	VGG-13 (BN)	300	1e-3	100, 200	0.1	1e-4	13	-
	VGG-16	300	1e-3	100, 200	0.1	1e-4	16	-
	VGG-16 (BN)	300	1e-3	100, 200	0.1	1e-4	16	-
	VGG-19	300	1e-3	100, 200	0.1	1e-4	19	-
	VGG-19 (BN)	300	1e-3	100, 200	0.1	1e-4	19	-
	ResNet-18	300	1e-3	100, 200	0.1	1e-4	18	-
	ResNet-34	300	1e-3	100, 200	0.1	1e-4	34	-
	ResNet-50	300	1e-3	100, 200	0.1	1e-4	50	-
	ResNet-101	300	1e-3	100, 200	0.1	1e-4	101	-
	DenseNet-161	300	1e-3	100, 200	0.1	1e-4	161	growth rate: 32
	DenseNet-169	300	1e-3	100, 200	0.1	1e-4	169	growth rate: 32
DenseNet-201	300	1e-3	100, 200	0.1	1e-4	201	growth rate: 32	

Table 19: The details of surrogate model set \mathcal{M} , which are used for the random selection of models in SWITCH_{rnd} and the generation of training data in Meta Attack. All ResNet networks are excluded in the experiments of attacking defensive models.

Defensive Model	Dataset	Attack	ASR	Avg. Query	Med. Query	Dataset	ASR	Avg. Query	Med. Query	Dataset	ASR	Avg. Query	Med. Query
ComDefend	CIFAR-10	NES	60.8%	1245	550	CIFAR-100	78%	727	300	TinyImageNet	74.8%	1326	500
		RGF	41.9%	2061	1173		66.7%	1723	816		43.7%	1855	765
		P-RGF	52.1%	2087	1115		78.4%	1523	630		48.8%	1986	866
		Meta Attack	19.6%	2363	1562		41.2%	2341	1173		9.2%	2173	1431
		Bandits	44.7%	1132	140		56.2%	297	22		52.4%	785	68
		PPBA	72.2%	720	103		95.3%	392	35		32.6%	569	73
		Parsimonious	99.1%	460	182		98.6%	218	86		91.6%	800	203
		SimBA	74.4%	783	218		84%	463	62		72.4%	1525	373
SWITCH _{rnd}	74%	413	6	77.2%	268	8	90.4%	238	8				
Feature Distillation	CIFAR-10	NES	54.5%	1474	450	CIFAR-100	77.6%	1071	250	TinyImageNet	33.7%	3325	2250
		RGF	44.4%	1717	768		62%	1208	408		9%	1619	765
		P-RGF	65.8%	1979	703		73.4%	1169	262		25.7%	2231	985
		Meta Attack	37.8%	2463	1560		54.4%	1813	912		3.7%	4187	2602
		Bandits	59.6%	736	96		80.9%	523	42		12.5%	1272	182
		PPBA	93.4%	702	90		97.5%	375	34		72.9%	1942	895
		Parsimonious	100%	193	107		100%	101	75		99.5%	359	193
		SimBA	86.4%	913	505		95.5%	482	89		47.1%	1509	647
SWITCH _{rnd}	93.4%	199	4	93.8%	162	3	81.3%	356	14				

Table 20: Experimental results of untargeted attack under ℓ_∞ norm on defensive models with the backbone of ResNet-50.

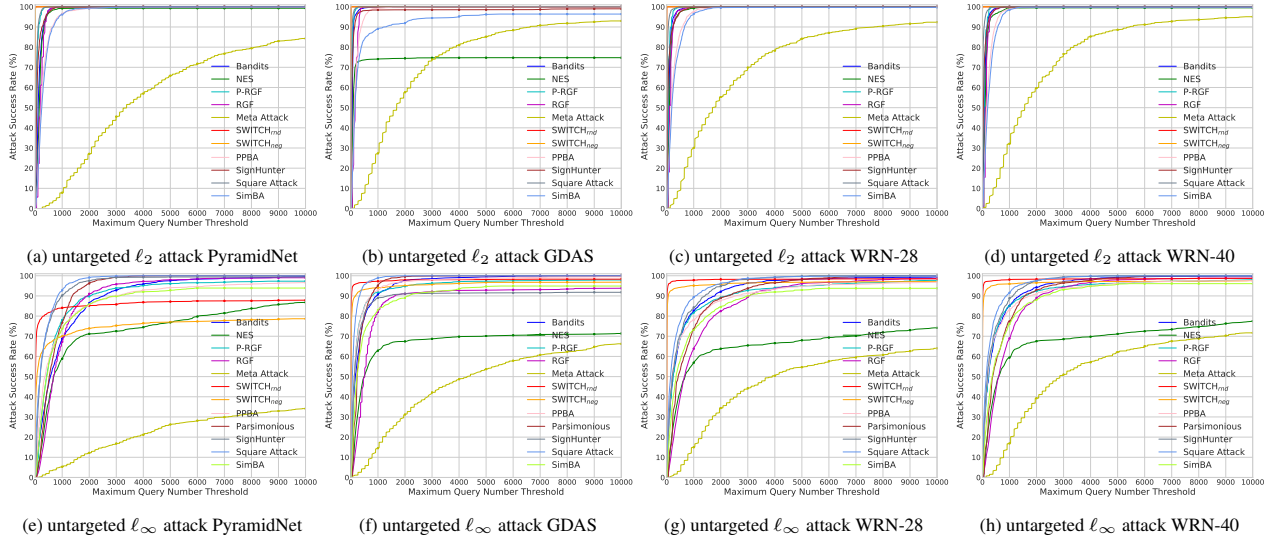


Figure 5: Comparison of attack success rate at different limited maximum queries using untargeted attack on CIFAR-10 dataset, where PyramidNet indicates PyramidNet-272.

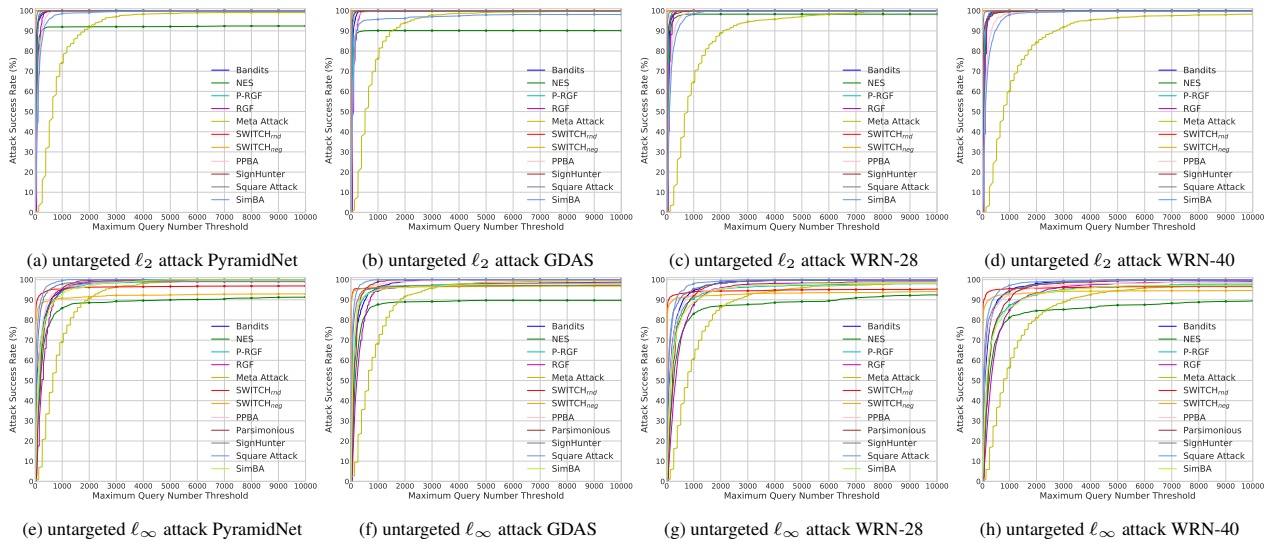


Figure 6: Comparison of attack success rate at different limited maximum queries using untargeted attack in CIFAR-100 dataset, where PyramidNet indicates PyramidNet-272

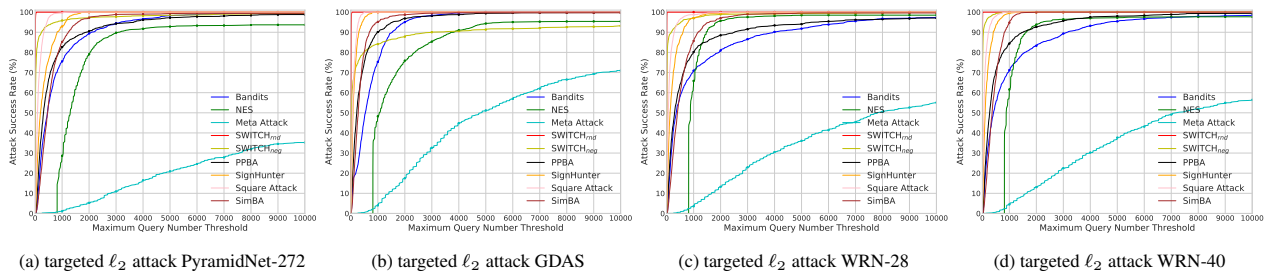
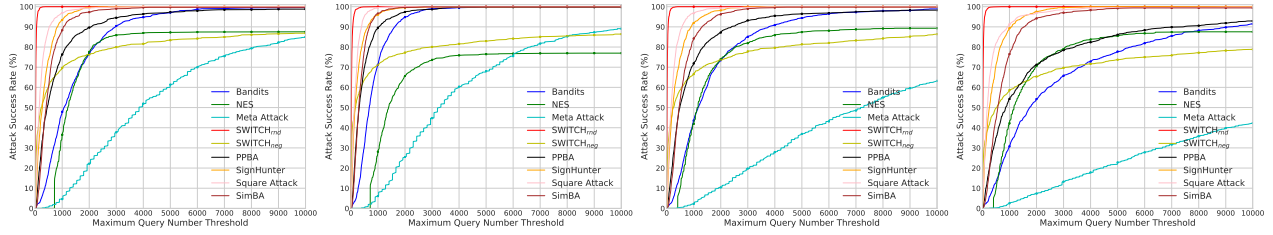
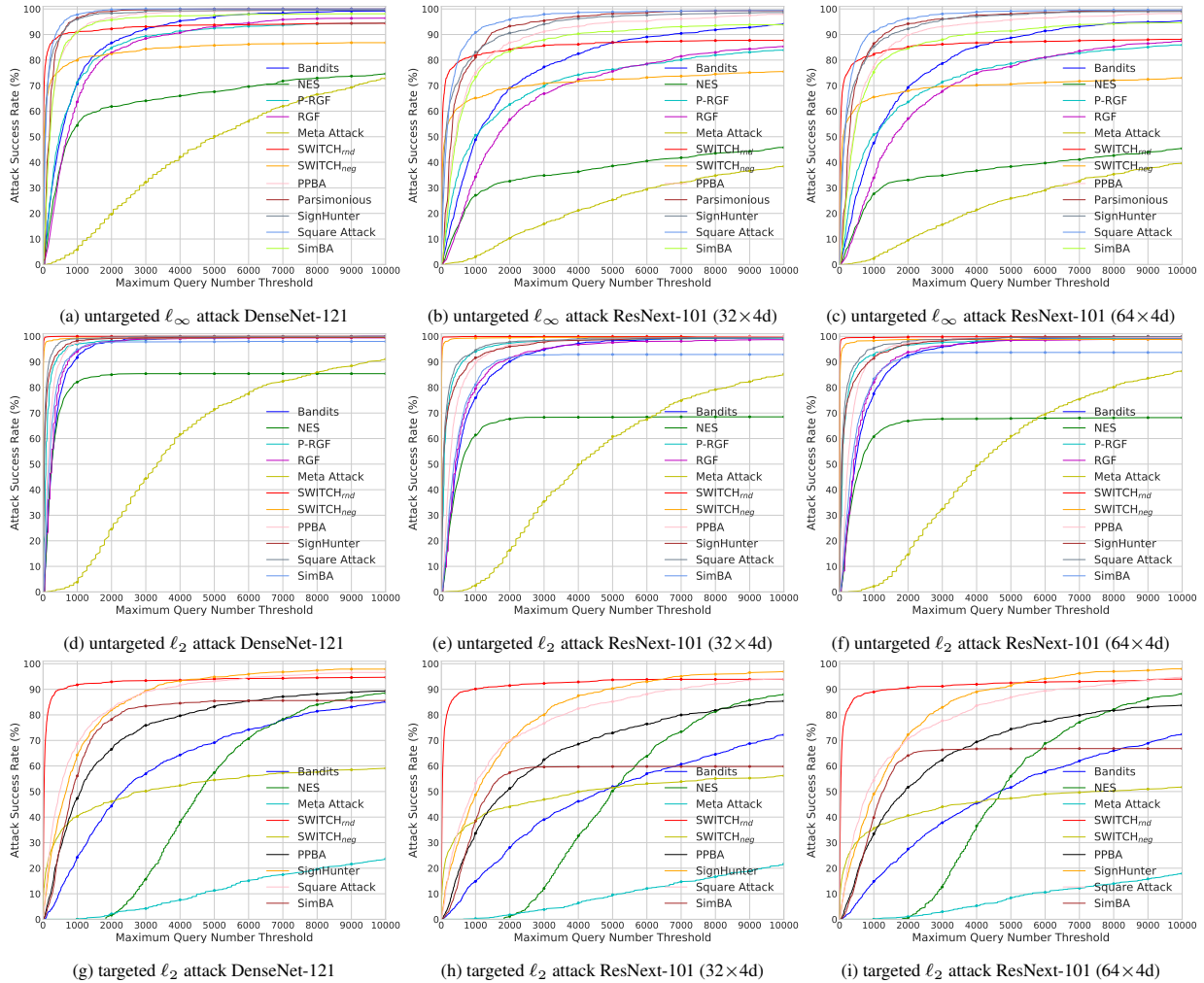


Figure 7: Comparison of attack success rate at different limited maximum queries using targeted attack in CIFAR-10.



(a) targeted ℓ_2 attack PyramidNet-272 (b) targeted ℓ_2 attack GDAS (c) targeted ℓ_2 attack WRN-28 (d) targeted ℓ_2 attack WRN-40
 Figure 8: Comparison of attack success rate at different limited maximum queries using targeted attack in CIFAR-100.



(g) targeted ℓ_2 attack DenseNet-121 (h) targeted ℓ_2 attack ResNext-101 (32x4d) (i) targeted ℓ_2 attack ResNext-101 (64x4d)
 Figure 9: Comparison of the attack success rate at different limited maximum queries in TinyImageNet dataset.

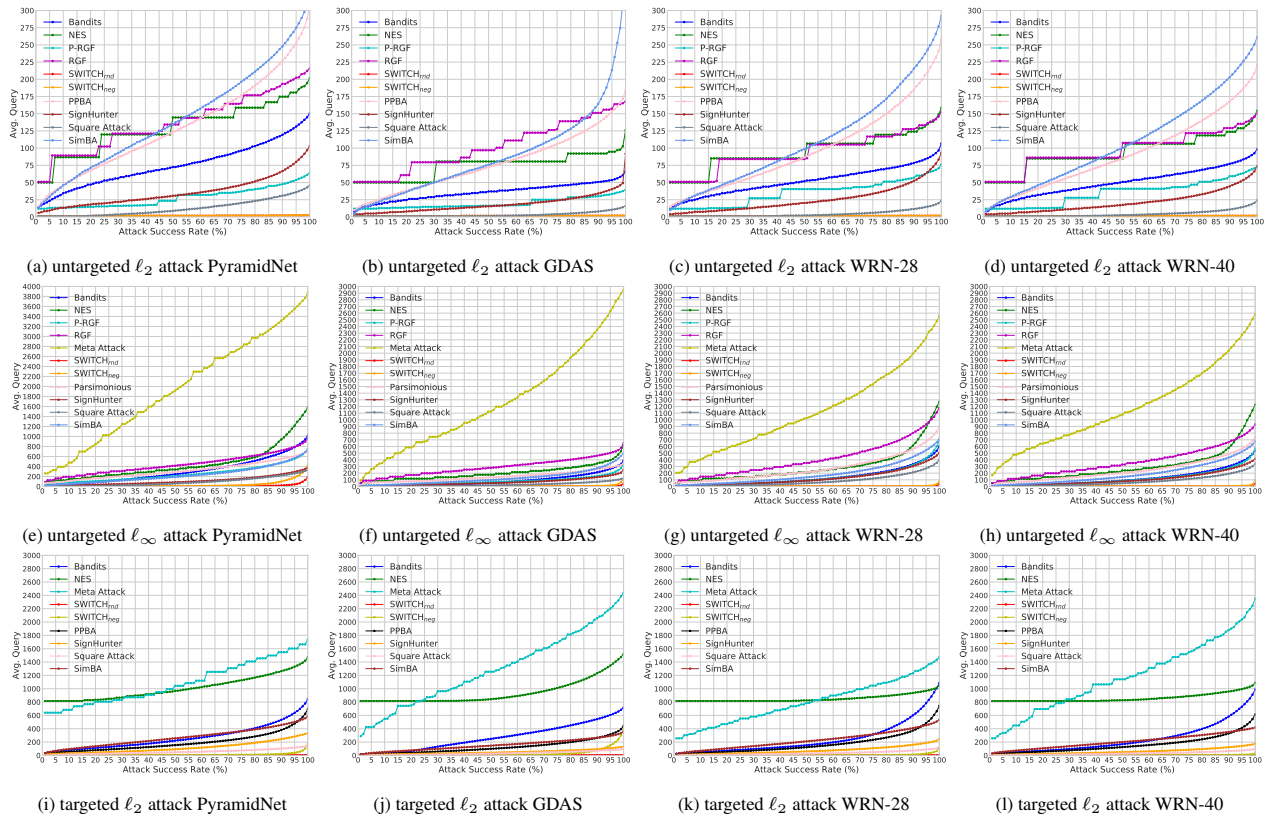
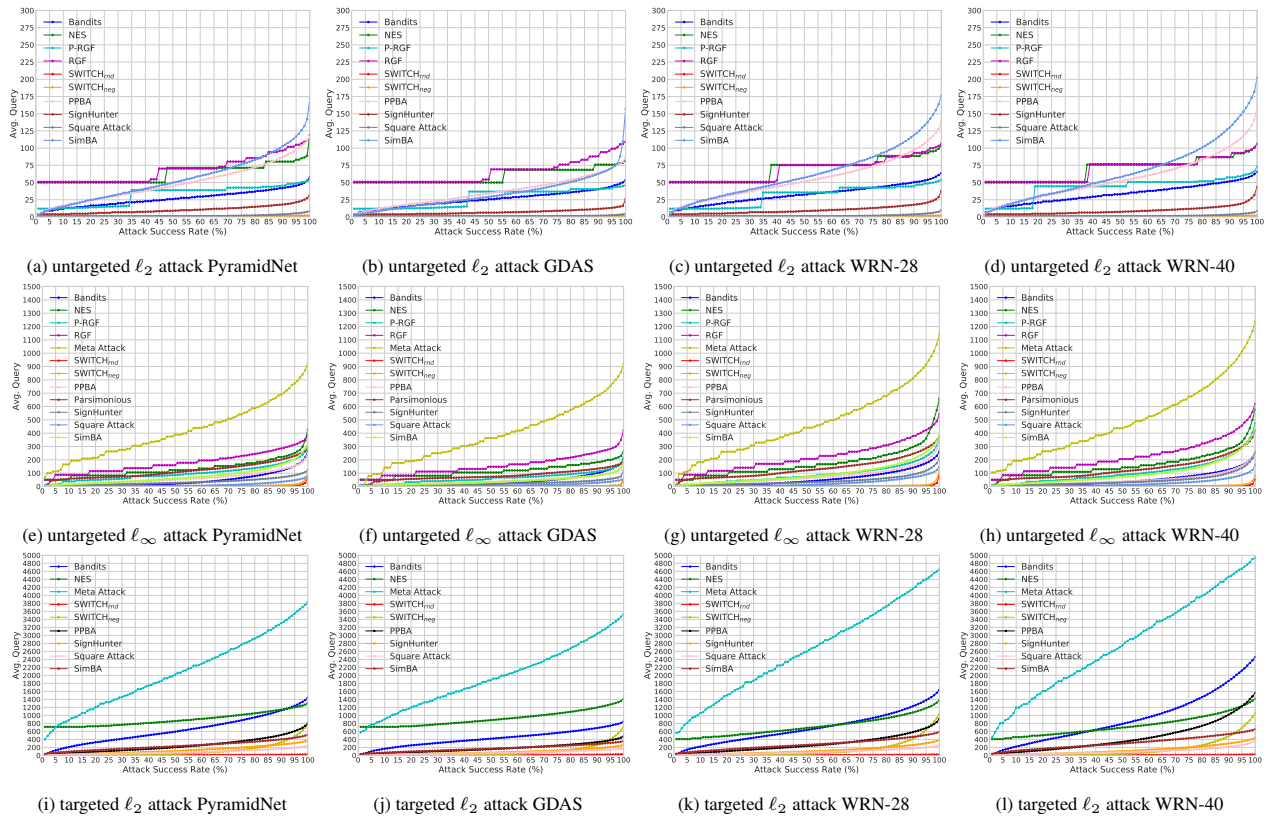


Figure 10: Comparison of the average query per successful image at different desired success rates in CIFAR-10 dataset, where PyramidNet indicates PyramidNet-272.



(a) untargeted ℓ_2 attack PyramidNet (b) untargeted ℓ_2 attack GDAS (c) untargeted ℓ_2 attack WRN-28 (d) untargeted ℓ_2 attack WRN-40
 (e) untargeted ℓ_∞ attack PyramidNet (f) untargeted ℓ_∞ attack GDAS (g) untargeted ℓ_∞ attack WRN-28 (h) untargeted ℓ_∞ attack WRN-40
 (i) targeted ℓ_2 attack PyramidNet (j) targeted ℓ_2 attack GDAS (k) targeted ℓ_2 attack WRN-28 (l) targeted ℓ_2 attack WRN-40
 Figure 11: Comparison of the average query per successful image at different desired success rates in CIFAR-100 dataset, where PyramidNet indicates PyramidNet-272.

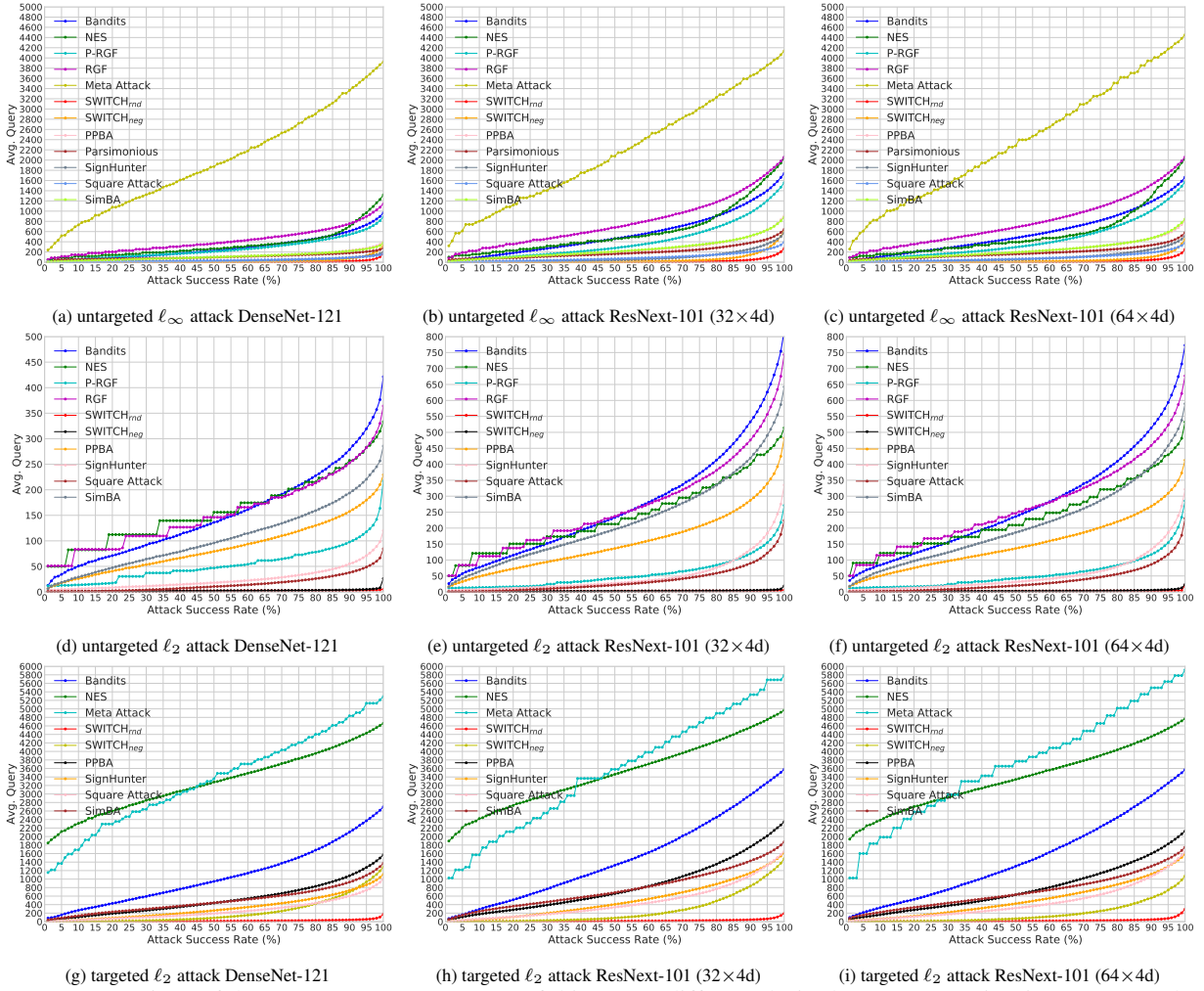
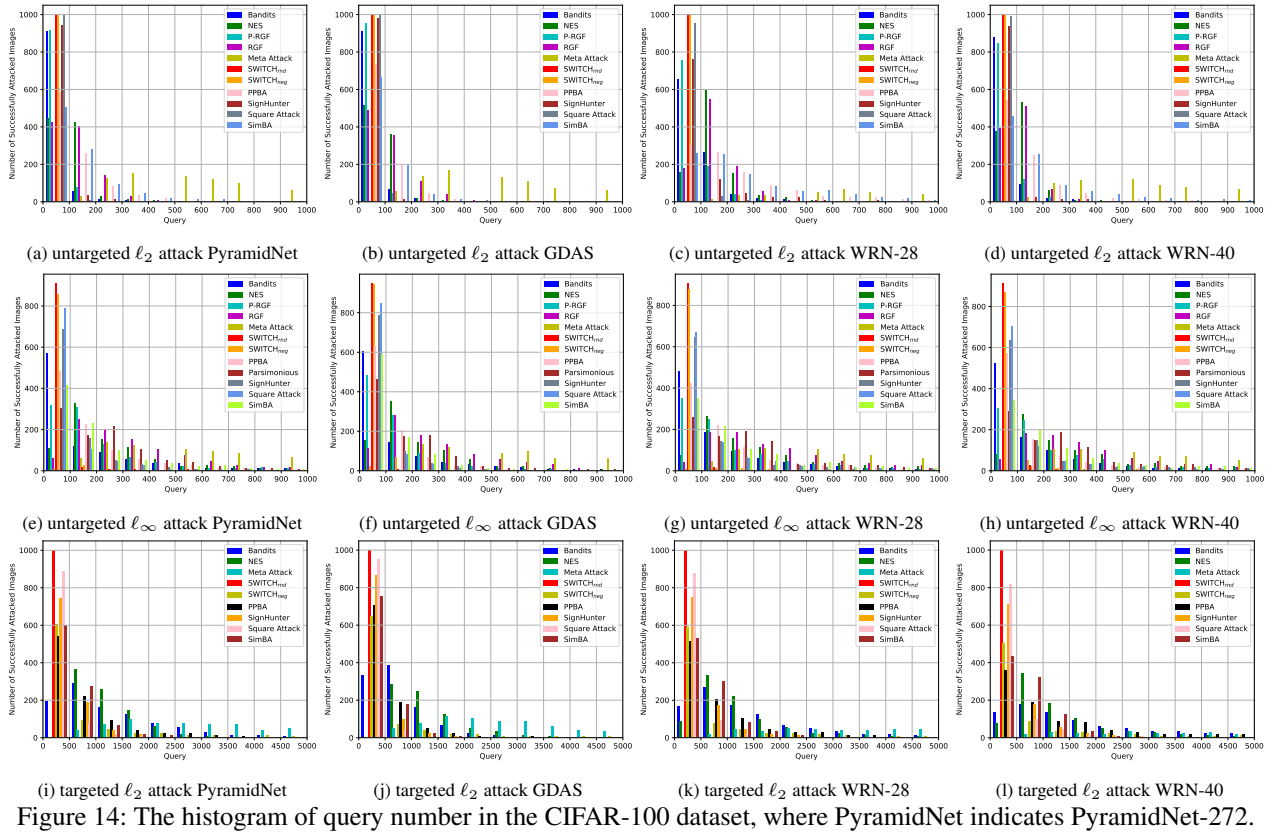
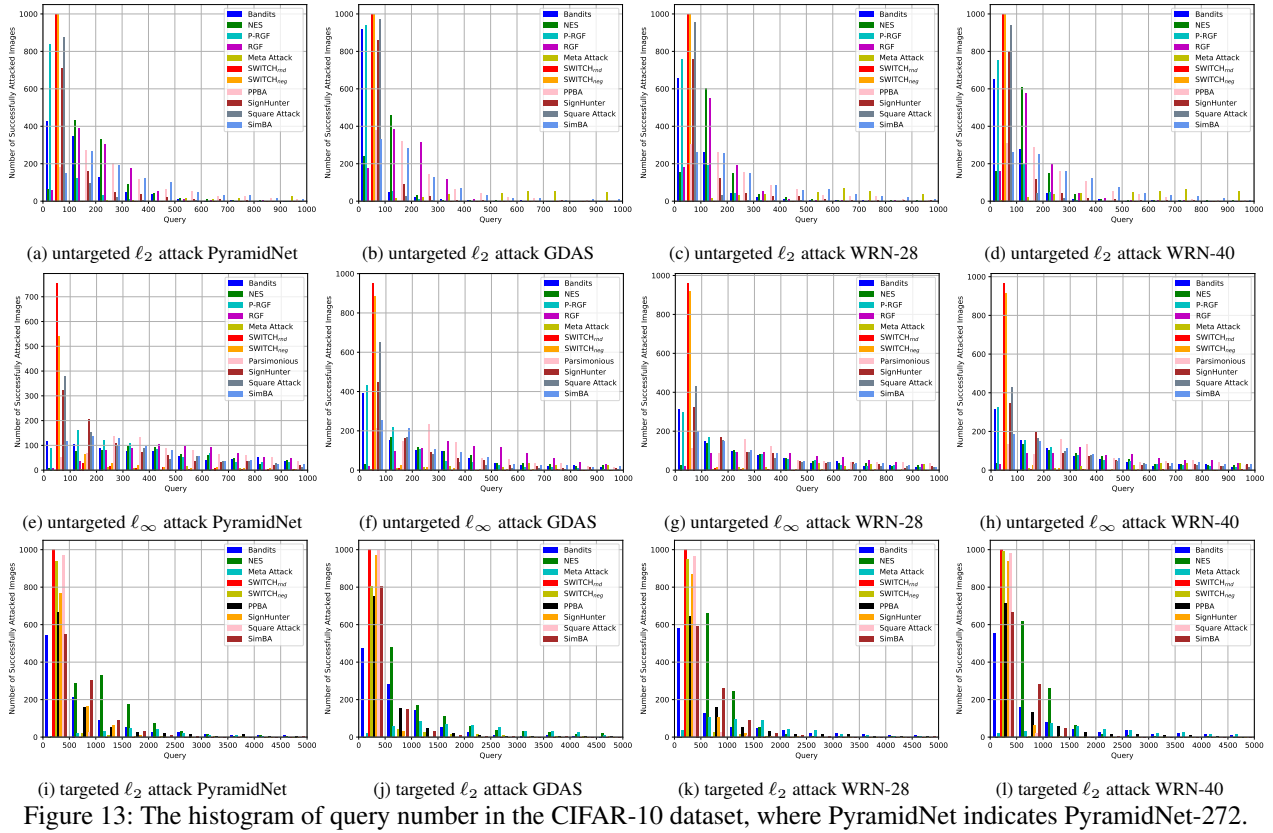


Figure 12: Comparison of the average query per successful image at different desired success rates in TinyImageNet dataset.



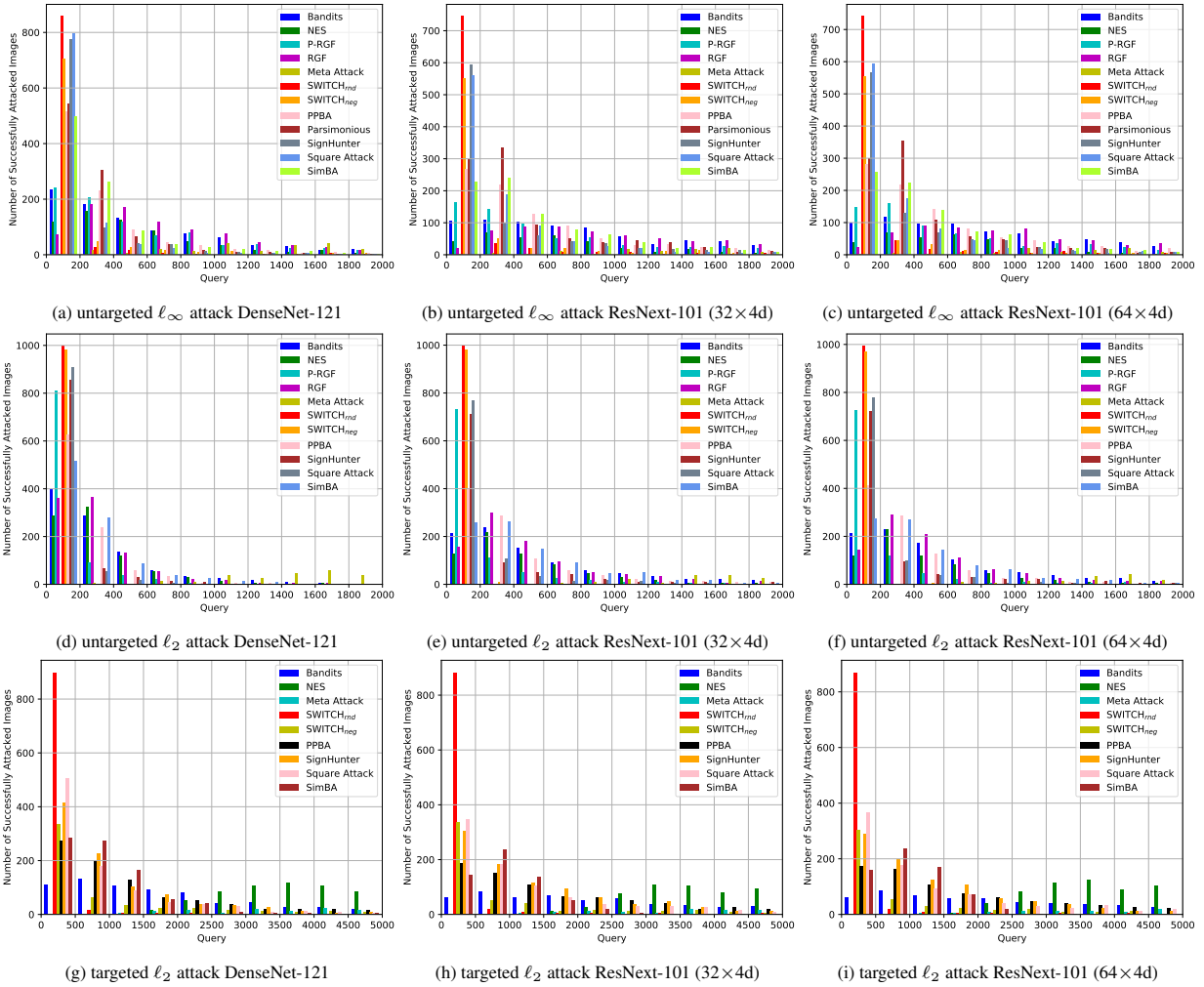


Figure 15: The histogram of query number in the TinyImageNet dataset.